Thesis for the degree of Doctor of Philosophy
in the Natural Sciences

Time-resolved X-ray diffraction and solution scattering studies of Sensory Rhodopsin II in isolation and in complex with its transducer

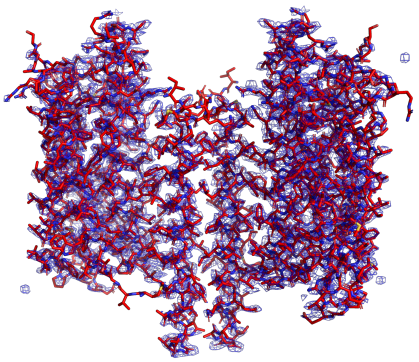

Giorgia Ortolani

UNIVERSITY OF GOTHENBURG

Department of Chemistry and Molecular Biology
Gothenburg, 2022

Thesis for the degree of Doctor of Philosophy
in the Natural Sciences

Time-resolved X-ray diffraction and solution scattering studies of the Sensory Rhodopsin II in isolation and in complex with its transducer

Giorgia Ortolani

Cover: Sensory Rhodopsin II in complex with its transducer HtrII. Structure solved at 2.85Å using serial synchrotron X-ray crystallography (SSX).

ISBN 978-91-8009-715-4 (Print)
ISBN 978-91-8009-716-1 (PDF)
Available online at http://hdl.handle.net

Department of Chemistry and Molecular Biology
Division of Biochemistry and Structural Biology
University of Gothenburg
SE-405 30, Göteborg, Sweden
Printed by Stema Specialtryck AB
Borås, Sweden, 2022

Abstract

Light is an important source of energy for many living organisms. Many life forms have therefore evolved cellular receptors that are able to sense light and thereby optimise conditions for photosynthesis and phototrophy. Microbial Rhodopsins are a family of heptahelical transmembrane proteins characterised by the presence of a retinal chromophore bound to a conserved lysine of helix seven. When the retinal absorbs a photon, it photoisomerises from an all-*trans* to a 13-*cis* conformation. Sensory Rhodopsin II (SRII) is a microbial rhodopsin identified in the halophilic archaeon *Nantronomonas pharaonis*. Together with its transducer protein HtrII, SRII it initiates a photophobic reaction of the host in response to blue light. Conformational changes within this complex are sensed by the HAMP domain of HtrII and trigger a signalling cascade controlled by the so-called two-component system (TCS). The TCS is ubiquitous in prokaryotes and is present in some eukaryotes. This implies significant pharmaceutical interest due to the involvement of TCS in bacterial virulence, antibiotic resistance, and phototaxis. Many details concerning the mechanisms of signal transduction through the SRII:HtrII complex remain unclear. In this work I aimed to address these questions by observing the nature and extent of secondary structural rearrangements in SRII in isolation and in complex with HtrII using time-resolved serial synchrotron X-ray crystallography (TR-SSX) and time-resolved X-ray solution scattering (TR-XSS). In PAPER I, we collected room-temperature TR-XSS data on SRII in isolation and compared the observed structural changes with those observed in bacteriorhodopsin (bR), a heavily studied light-driven proton pump. Our observations provide structural insight into why these very similar proteins have very different photocycle duration. In both proteins, helix F undergoes an outward movement, yet structural rearrangement within helix G are suppressed in SRII, resulting in a slower photocycle and reflecting its function as a signalling receptor. In PAPER II we observed the structure of the SRII:HtrII complex at room-temperature using serial synchrotron x-ray crystallography (SSX). Our data provides

the first room-temperature structure of the SRII:HtrII complex and allows five additional residues to be modelled on the cytoplasmic side of transmembrane helix 1 (TM1) of HtrII. In Paper III we used TR-SSX to investigate light-initiated conformational changes of within the SRII:HtrII complex. Our observations show how a structural signal originating at the retinal is transferred from SRII to HtrII. A preliminary structural analysis suggests that an outward movement of helix F of SRII is translated into a piston-like movement of transmembrane helix 2 (TM2) towards the cytoplasm, a model that is largely consistent with the conclusions of earlier cryo-trapping studies. In Paper IV we used TR-XSS to analyse conformational changes in SRII and the SRII:HtrII complex. As a solution phase method, TR-XSS is complementary to crystallography and protein motions are not constrained by a crystal lattice, but the information content is lower. Our TR-XSS data were consistent with a light-induced outward movement of the cytoplasmic portions of helices E and F, and more subtle movements in helices C, D and E. Structural rearrangements in helices E and F are less extensive when the transducer binds to SRII. These results increase our understanding of how a light signal is sensed by the phototaxis receptor SRII, and how this signal is transmitted to its transducer protein, HtrII.

Sammanfattning på svenska

Ljus är en viktig energikälla för många levande organismer. Många arter har därför utvecklat cellulära receptorer som kan känna av ljus och därmed optimera förutsättningarna för fotosyntes och fotoautotrofi. Mikrobiella rodopsiner är en familj transmembranösa proteiner i hepta-helix-form, som karakteriseras av närvaron av retinal kromofor bundet till ett konserverat lysin i den sjunde helixen. När retinal absorberar en foton, sker en foto-isomerisering från all-*trans* till 13-*cis*-konformation. Sensoriskt rodopsin II (SRII) är ett mikrobiellt rodopsin som finns i den halofila archeon *Nantronomonas pharaonis*. Tillsammans med transducerar- proteinet HtrII, initierar SRII en fotofobisk reaktion i sin värd som svar på blått ljus. Strukturella förändringar i detta komplex detekteras sedan av HAMP-domänen i HtrII och initierar en kaskad av signaler som kontrolleras av det så kallade tvåkomponent-systemet (TCS). Detta system är allmänt förekommande i prokaryoter och förekommer även i vissa eukaryoter. Då TCS påverkar faktorer såsom bakteriell virulens, antibiotikaresistens och fototaxis, är en ökad kunskap om detta system av stort intresse i många farmaceutiska sammanhang. Vi saknar dock fortfarande kunskap om många detaljer kring SRII:HtrII-komplexet och dess signalsystem. Syftet med denna avhandling var därför att adressera dessa frågor genom att studera strukturen av SRII ensamt och i komplex med HtrII genom att använda tidsupplöst seriekristallografi (TR-SSX) och tidsupplöst röntgenspridning (TR-XXS).

I projekt 1 samlade vi in rumstemperatur-TR-SSX-data från isolerat SRII och jämförde de observerade strukturella ändringarna med de som observerats i bakterierodopsin (bR), vilket är en välstuderad ljusdriven protonpump. Våra observationer ger strukturell insikt i varför dessa mycket lika proteiner har väldigt olika längd på fotocykeln. Helix F genomgår en utåtvänd rörelse i båda dessa proteiner, men ändå är omstruktureringen i helix G hämmad i SRII. Detta resulterar i en långsammare fotocykel, vilket i sin tur speglas i dess funktion som signalreceptor.

I projekt II studerade vi strukturen av SRII:HtrII-komplexet med seriekristallografi (SSX). Våra resultat visar den första strukturen av SRII:HtrII-komplexet i rumstemperatur. Vi kunde dessutom modellera ytterligare fem aminosyror i den cytoplasmiska delen av den transmembranösa helixen 1 (TM1) i HtrII, vilket inte tidigare gjorts.

I projekt III använde vi SSX för att studera ljusaktiverade strukturella förändringar i SRII:HtrII-komplexet. Våra resultat visar hur en strukturell signal från retinal överförs från SRII till HtrII. En preliminär strukturell analys indikerar att en utåtgående rörelse av helix F i SRII överförs till en pistong-lik rörelse i den transmembranösa helixen 2 (TM2) mot cytoplasman, vilket stödjer tidigare studier.

I projekt IV använde vi TR-XSS för att studera strukturella förändringar i SRII och SRII:HtrII-komplexet. Då TR-XSS är en metod för att studera proteiner i lösning, fungerar denna som komplement till kristallografi och proteinrörelser är då inte begränsade av kristallstrukturen, men informationsinnehållet är lägre. Vår TR-XSS data stödjer en ljusaktiverad utåtgående rörelse av den cytoplasmiska delen av helixar E och F, och subtila rörelser i helixarna C, D och E. De strukturella ändringarna i helix E och F är mindre omfattande när transduceraren binder till SRII. Dessa resultat ökar vår förståelse för hur ljus som träffar fototaxis-receptorn SRII initierar en signal och hur denna signal överförs till HtrII.

Acknowledgements

Thank you to **Richard** and **Gisela** for taking me as part of this group. All the amazing experiences I had during these years will be with me forever. Thank you **Sebastian** for taking care of burocracy. **Michal, Kristina, Gergely, Johanna, Björn and Julia**, it has always been pleasant to talk with you during lunch, or in the corridors.

In our group, our projects are strongly connected to each other and all of them require a lot of team effort, especially during extenuating beam-times where the reciprocal emotional support is fundamental. Thank you to **Cecilia Wickstrand**, even if we haven´t had the opportunity to work very close, I really appreciated all our discussions and your hints on the Channelrhodopsin 2 project. **Rob Dods** thank you for welcoming me on the first weeks of my PhD and for introducing me to the fantastic world of protein purification. **Rob Bosman** for the crazy long working hours, the fun, and for the never ending nerdy conversations. I am very happy I met you. **Lucija**, I really don´t know how I could finish my PhD without you!!! You have given me a lot of joy and support during our time together. Thank you for staying positive even in the hard lab times. **Per** for being a friend and also the coolest and nerdiest office mate in the world, and for always being there for a talk or for a good advice. **Analia** for bringing a huge smile to my face every time I saw you. I loved talking with you, and I enjoyed and all the positivity I got from you even if all the sample was lost and nothing was working in the lab. **Adams** for the inestimable help with every problem related to programming, even if it was not work related, and even during nights/holidays/sick leaves/weekends. **Greger** for the many nice beam-times and conversations we had whenever we met, and for the emotional support especially on the last beam-time. **Swagatha**, for becoming more and more a person I could rely on, and for sharing your thoughts that were often the same as mine. Stay strong and don't give up! **Petra Båth**, for all the interesting discussions and sharing experience when it comes to work in the lab and for making me discover corean boybands and the shuffling. **Sarabi** we haven´t seen you around much in the last years, so good luck for your future. **Tinna** for

having a huge patience with me when I was writing grumpy emails, and for being a huge and reliable support for part of my work. Thank you to **Cecilia Safari** for always being sweet and supportive, to **Rajiv** for making me discover that my patience was better than I thought, and for all the laughs during the beamtimes. Thank you **Andrea** for the psychological support group we created together with Lucy, **Florian** for sharing with me a huge amount of common interests. **Majo**, **Ann** and **Arpitha**, I liked you from the first instant, and I hope we will keep contacts in the future. You are the sweetest person I have ever met. **Dimitra** and **Weixiao**, we haven´t had many opportunities to talk, but I wish you luck for your future. Thank you to **Bruno and Lars** for the enormous technical support, and for the nice conversations. **Katharina**, it has been lovely to share the Soapbox experience with you. I hope there will be more opportunities like this in the future. **Atsarina**, I love your sense of humour! Johanna´s group **Davide, Jack, Lisa, Vajradhar**, Gisela's group, **Jonathan, Doris, Andreas, Owens, Emil**, Julia's group **Micaela and Leona**, Michal's group **Himanshu, Dylan**, Sebastian's group **Amke, Leocadie, Jennifer, Lidja**, Gergely's group **Viktor, Maja**, Kristina's group **Jessica** good luck for your future! Björn's group **Emilie, Darius, Johannes, Ashish, Irena, Damasus, Ylber, Jens, Hannah, Filippo**, it is always nice to hang out. You should come upstairs more often!

I am sure I have forgotten a lot of new entries in the lab. To all the new ones arriving: welcome to Lundberg lab!!! Enjoy the ride!!!

Thank you to my **family**, mamma, papá, Valerino, Margheritina, nonna Antonietta, zii, zie, cugino e cugine. Yes, italian families are big! E pure questa è fatta!!! Grazie in particolare grazie ai miei zii e alle mie zie per aver sempre creduto in me e per essere stati delle grandi guide. Thank you to **Peter** for loving me, understanding me, encouraging me and supporting me when I felt not good enough, and to **Gloria** for being the wonderful person you are and for your inestimable support.

To **Carlo** for supporting me and for showing me how proud you are of me. **Marianne, Martina and Giulia** for loving me and supporting my dreams but also criticising me in productive ways when needed. **Vinicio, Medea, Alessandro, Valerio ed Eleonora**, you are distant in space, but I have you in my heart. **Viviana**, for being the strong woman you are, and for sharing with me your feelings and showing me your support when we

were struggling for the same things in the same time. You are precious and I am sure your future will bring you a lot of success. **Ebba** and **Katchu**, for understanding when I was going to a rough time and being there no matter what, and a special hug goes to **Antonia**. We don´t meet often, but for me it is always as we met the day before.

Publications

This thesis consists of the following research papers:

PAPER I: Robert Bosman, **Giorgia Ortolani**, Swagatha Ghosh, Daniel James, Per Börjesson, Greger Hammarin, Tinna Björg Úlfarsdóttir, Tobias Weinert, Florian Dworkowski, Tomizaki Takashi, Jörg Standfuss, Gisela Brändén, Richard Neutze **"Structural basis for the prolonged photocycle of Sensory Rhodopsin II revealed by serial synchrotrons crystallography."** Submitted manuscript.

PAPER II: **Giorgia Ortolani**, Robert Bosman, Lucija Ostojic, Tinna Björg Úlfarsdóttir, Swagatha Ghosh, Daniel James, Jack B. Greisman, Kevin M. Dalton, Greger Hammarin, Per Börjesson, Tobias Weinert, Florian Dworkowski, Takashi Tomizaki, Doeke R. Hekstra, Joerg Standfuss, Gisela Brändén, Richard Neutze **"Serial synchrotron crystallography structure of the Sensory Rhodopsin II:transducer complex."** Manuscript.

PAPER III: **Giorgia Ortolani**, Robert Bosman, Lucija Ostojic, Jack B. Greisman, Kevin M. Dalton, Adams Vallejos, Tinna Björg Úlfarsdóttir, Swagatha Ghosh, Daniel James, Greger Hammarin, Per Börjesson, Tobias Weinert, Florian Dworkowski, Takashi Tomizaki, Joerg Standfuss, Doeke R. Hekstra, Gisela Brändén, Richard Neutze **"Serial crystallography structure of the light-activated Sensory Rhodopsin II:transducer complex."** Manuscript draft.

PAPER IV: Daniel Sarabi*, Robert Bosman*, Lucija Ostojić, Swagatha Ghosh, **Giorgia Ortolani**, Matteo Levantino, Martin Nors Pedersen, Mathias Sander, Petra Båth, Greger Hammarin, Robert Dods, Per Börjesson, Cecilia Safari, Michael Wulff, Gisela Brändén, Richard Neutze **"Time-resolved X-ray solution scattering observations of light induced structural changes in Sensory Rhodopsin II."** Manuscript.

Note: The authors whose name is signed by an asterisk have equally contributed to the study.

Related papers that I have co-authored but that are not included in this thesis:

PAPER V: Daniel Sarabi*, **Giorgia Ortolani***, Cecilia Wickstrand, Lucija Ostojić, Swagatha Ghosh, Robert Bosman, Martin Nors Pedersen, Mathias Sander, Petra Båth, Robert Dods, Greger Hammarin, Cecilia Safari, Matteo Levantino, Michael Wulff, Gisela Brändén, Richard Neutze **"Time-resolved x-ray solution scattering studies of structural changes in Channelrhodopsin 2."**. Manuscript

PAPER VI: C. Safari, R. Andersson, S. Gosh, J. Johannesson, P. Båth, R. Bosman, P. Dahl, E. Nango, R. Tanaka, E. Dunevall, P. Börjesson, O. Uwangue, D. Zoric, G. Hammarin, M. Panman, E. Svensson, **G. Ortolani**, T. Tanaka, T. Tosha, H. Takeda, H. Naitow, T. Arima, A. Yamashita, M. Sugahara, T. Nakane, O. Nureki, S. Iwata, R. Neutze and G. Brändén. **"Room-temperature structure of CO-bound ba3-type cytochrome c oxidase reveals mechanistic differences between A-type and B-type enzymes."** Manuscript (2020).

PAPER VII: Petra Båth, Analia Banacore, Per Börjesson, Robert Bosman, Cecilia Wickstrand, Cecilia Safari, Robert Dods, Swagatha Ghosh, Peter Dahl, **Giorgia Ortolani**, Tinna Björg Ulfarsdottir, Greger Hammarin, María-José García Bonete, Adams Vallejos Donoso, Lucija Ostojic, Petra Edlund, Johanna-Barbara Linse, Elin Dunevall, Rebecka Andersson, Eriko Nango, Shigeki Owada, Rie Tanaka, Takanori Nakane, Ayumi Yamashita, Kensuke Tono, Yasumasa Joti, Tomoyuki Tanaka, Toshi Arima, Osamu Nureki, Daniel James, Karol Nass, Philip Johnsson, Gregor Knopp, Dmitry Ozerov, Claudio Cirelli, Christopher Milne, So Iwata, Gisela Brändén, Richard Neutze. **"Lipidic cubic phase serial femtosecond crystallography structure of a photosynthetic reaction centre"**.

Acta Crystallographica (2022). D
https://doi.org/10.1107/S2059798322004144

PAPER VIII: T. Gruhl, T. Weinert, M. Rodrigues, C. J. Milne, **Giorgia Ortolani**, K. Nass, E. Nango, S. Sen, P. J M Johnson, C. Cirelli, A. Furrer, S. Mous, P. Skopintsev, D. James, F. Dworkowski, P. Baath, D. Kekilli, D. Ozerov, R. Tanaka, I. Martiel, C. Bacellar, S. Brünle, C. M. Casadei, A. D. Diethelm, D. Gashi, H. Glover, G. Gotthard, Y. Joti, G. Knopp, E. Lesca, P. Ma, J. Muehle, S. Owada, F. Pamula, D. Sarabi, O. Tejero, C. Tsai, N. Varma, A. Wach, W. Wu, S. Boutet, K. Tono, P. Nogly, X. Deupi, S. Iwata, R. Neutze, J. Standfuss, G. Schertler, V. Panneels. **"Ultrafast structural changes direct the reaction pathway of vision"**. Manuscript under review.

Note: The authors whose name is signed by an asterisk have equally contributed to the study.

Contribution report

PAPER I: I contributed to the improvement of the protocols, produced cells, executed protein purification and crystallisation. I participated in the data collection. I helped with the manuscript and the submission of the PDBs.

PAPER II: I improved the protocols, produced cells, executed protein purification and crystallisation. I collected and processed data. I wrote the manuscript and created the figures.

PAPER III: I improved the protocols, produced cells, executed protein purification and crystallisation. I collected and processed data. I wrote the manuscript and created part of the the figures.

PAPER IV: I participated in the data collection.

Abbreviations

Here follows a list and short explanation of the different abbreviations used in this thesis.

bR	**b**acterio**R**hodopsin
EPR	**E**lectron **P**aramagnetic **R**esonance
HAMP	**H**istidine kinases **A**denylate cyclases **M**ethyl accepting proteins and **Phosphatases** Domain
HtrII	Halobacterial integral membrane transducer protein
LCP	**L**ipid **C**ubic **P**hase
PDB	**P**rotein **D**ata **B**ank
Ret	Retinal
SEC	**S**ize **E**xclusion **C**hromatography
SLS	**S**wiss **L**ight **S**ource (third-generation synchrotron light source at the Paul Scherrer Institut in Switzerland)
SRII	**S**ensory **R**hodopsin **II**
TCS	**T**wo **C**omponent **S**ignalling
TM	**T**rans **M**embrane (protein domain)
TR-SSX	**T**ime**R**esolved- **S**erial **S**ynchrothron **x**-ray crystallography
TR-XSS	**T**ime**R**esolved- **X**-ray **S**olution **S**cattering
X-FEL	**X**-Ray **F**ree-**E**lectron **L**aser
Å	**Å**ngstrom

Contents

List of Figures

To Zoe...

Chapter 1

Introduction

Proteins are biological macromolecules composed by sequences of amino acids bound together through peptide bonds. Proteins are essential for all living organisms. They have key functions in cellular processes, metabolism, DNA replication and modification, transcription, translation, intracellular signalling, cell-cell communication, protein folding and degradation, transport, cytoskeletal and structural, defence and immunity, and more [1], [2].

Structural biology is a multidisciplinary field where the structure of macromolecules like proteins or nucleic acids can be studied at atomic level. This field includes disciplines like molecular biology, biochemistry and biophysics. Through the use of biophysical techniques such as nuclear magnetic resonance, electron microscopy, and crystallography, biological molecules can be observed both in their inactive state and in their dynamic states. Structural biology is based on the strong connection between the structure of a protein and its function. For that reason, by observing a protein in its three-dimensional conformation, and knowing its chemical and physical characteristics, we can understand its function and how this task is performed [3].

This thesis presents my studies on the structure and conformational changes of photo-active membrane proteins belonging to the microbial rhodopsin family such as Sensory Rhodopsin II (SRII), and Sensory Rhodopsin II in a complex with its transducer HtrII (SRII:HtrII). SRII:HtrII is involved in the *Two-component signalling system*, important in regulating photophobic reactions in *Natronomonas pharaonis*. SRII in isolation and with its cognate transducer have been observed both in their ground state and in

their photoactive state using time-resolved serial synchrotron X-ray crystallography (TR-SSX) and time-resolved solution scattering (TR-XSS).

1.1 Biochemistry of proteins, an overview

Proteins are important macromolecules essential for all living organisms. They are composed of 20 amino acids linked together by peptide bonds. The general structure of an amino acid (Fig.1.1) consists of a central carbon atom (-C-) where the basic amino group (-NH_2) and the acid carboxyl group (-COOH) are attached at the two poles. Attached to the remaining sides, a side chain (-R), unique to each amino acid, that assesses the chemical characteristics of the amino acid itself (e.g. pH, polarity), and a hydrogen atom [4].

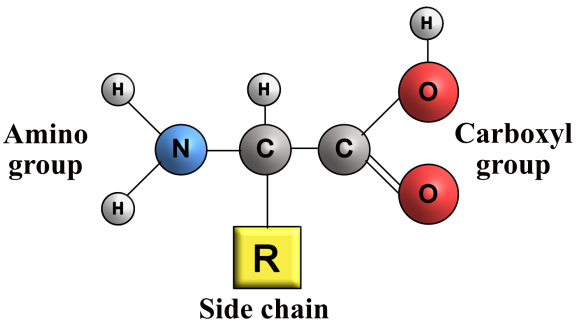

Figure 1.1: Example of an amino acid

Each of these structural units is bound to the others through peptide bonds. A peptide bond is a chemical bond that links the carboxyl group of an amino acid with the amino group of the adjacent amino acid. When these bonds form, one molecule of water is released, giving rise to a long polypeptide chain that can assemble itself into three-dimensional structures. The protein 3D-structure is organised on many levels of complexity and it is held in place by hydrogen bonds, ionic bonds, and Van der Waals interactions. Protein conformations are called primary, secondary, tertiary and quaternary structures. The primary structure of a protein is composed

of a polypeptide chain, the secondary structure is helped by hydrogen bonds and consists of structures like α-helices and β-sheets. The tertiary structure is held in place by non-covalent bonds where the α-helices and β-sheets are arranged together in a more complex structure, and the quaternary structure implies the presence of two or more polypeptides bound together [5].

1.2 Cellular membrane and membrane proteins

The cellular membrane is a physical barrier that confers protection to the cell from the extracellular environment, preserving the stability of the intracellular environment. In order to understand how it is able to selectively control the passage of ions and large molecules in and out of the cell in a controlled manner, it is fundamental to understand its structure.

According to the *Fluid mosaic model* [6], a typical cell membrane is organised as a phospholipid bilayer as described in figure 1.2.

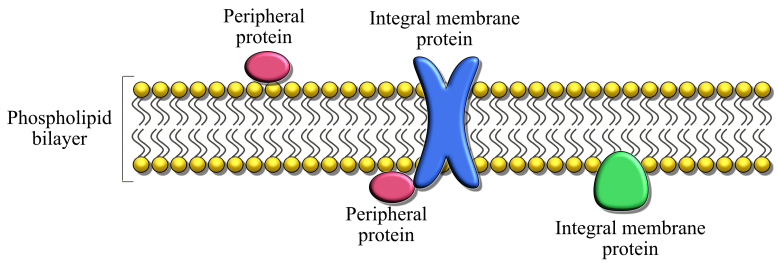

Figure 1.2: Phospholipid bilayer with peripheral and integral membrane proteins.

A phospholipid bilayer is a structure in which an ensemble of phospholipids (amphipathic molecules having a polar hydrophilic head made of phosphate and glycerol, and hydrophobic saturated and unsaturated fatty acid tails) are ordered in two layers where the heads point towards the surface of the membrane and the tails point towards the centre [6]. In addition, steroles are located within the polar heads of the phospholipids

and inside the double layer. Glycoproteins and glycolipids are on the outer side of the membrane exposing their bound carbohydrate portions [7]. The location of the proteins in the the phospholipid bilayer can vary based on their structural, chemical, and physical characteristics.

Membrane proteins enable the cell to receive signals from the extracellular matrix and allow different signalling molecules or ions to pass through it in both directions [7]. They are grouped into two main categories: *peripheral* and *integral membrane proteins*. *Peripheral proteins* are surface proteins located on both the cytosolic and the extracellular sides of the bilayer. They don't interact directly with the hydrophobic part of the phospholipid bilayer but instead they are non-covalently bound to either the polar heads of phospholipids, or the integral membrane proteins. Integral membrane proteins are strongly attached to the membrane. They can be lipid-anchored proteins and interact with the polar heads of the phospholipids by a covalently attached hydrocarbon chain, or they can be transmembrane proteins and cross the whole phospholipid bilayer with one or more of their domains, usually α-helices [5].

Small and uncharged molecules can diffuse through the phospholipid bilayer, however, the bigger and more polar the molecules and ions are, the more their diffusion becomes complex. *Integral membrane proteins* play an important role in allowing big polar molecules and charged ions to cross the cell membrane. These proteins select and transport them through the cellular barrier and regulate the associated cellular processes [8].

Transport through the membrane is classified as *passive* or *active*. In the *passive transport*, water and ions can freely move towards a lower gradient, while amino acids need to be carried to move towards a lower gradient. When the molecule of interest needs to move against the gradient, then *active transport* occurs at the expense of energy as ATP, or by coupling the transport with another molecule that moves towards a lower gradient using the same transporter [7].

1.3 Rhodopsin family

Rhodopsins (Fig.1.3A) are widely distributed light-activated integral membrane proteins responsible for transport and signalling across the cell membrane. They are activated by light thanks to a retinal chromophore bound to their seventh transmembrane helix, and they can function as ion transporters, sensory receptors, and channels [9]–[11]. They are divided into Type 1 (microbial rhodopsins) and Type 2 (animal rhodopsins).

Type 2 rhodopsins can be found in a variety of animals with vision, including humans. Human rhodopsin is present in cone and rod cells in the retina, where they control the transmembrane ion flux responsible for visual phototransduction, by coupling with G-proteins [12]. *Human* rhodopsin, like many type 2 rhodopsins, is a G-protein-coupled receptor (GPCR) [13]. One of the biochemical characteristics that make them different from type 1 is the presence in the animal rhodopsins of the 11-*cis*-retinal ligand attached to the lysine residue on the seventh transmembrane helix that upon photon absorption isomerises from 11-*cis*-retinal to all-*trans*-retinal. Upon photoactivation, they are able to catalyse either the GDP/GTP exchange in the heterotrimeric G proteins ($G\alpha\beta\gamma$) or the arrestin-mediated signalling [14].

Type 1, or Microbial rhodopsins, are found in archaea, eubacteria, fungi, and algae [15]. They function as pumps, channels, and light-sensors. They are regulated by light and their spectrum of absorption is within the visible region (400 to 700 nm). The better known microbial rhodopsins are shown in figure 1.3C and they are halorhodopsin (HR), which transports one chloride anion per photon inward across the cell membrane, and bacteriorhodopsin (bR), which translocates protons and consequently generates a transmembrane gradient which is harvested by ATP-synthase [16]. Moreover Channelrhodopsin (ChR) is a nonspecific cation channel [17], and Sensory Rhodopsin II (SRII) and Anabaena Sensory Rhodopsin (ASR) are light sensors [14], [18]. All the microbial rhodopsins share a conserved motif having 7 transmembrane (7TM) alpha helices as shown in figure 1.3A, the C-terminus on the cytoplasmic side and the N-terminus in the extracellular side [19]. The retinal cofactor is attached to a lysine with a covalent bond through a protonated Schiff base [15]. The Retinal, shown in figure 1.3B also known as vitamin A, is a molecule derived from

beta-carotene that isomerises from all-*trans* to 13-*cis*-retinal upon light stimuli.

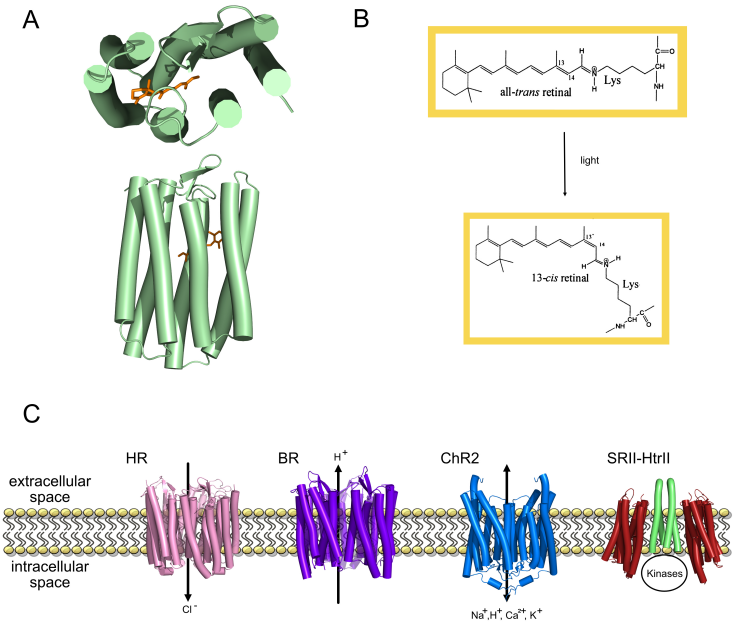

Figure 1.3: Microbial rhodopsins. A) The common rhodopsin structure having 7 α-helices and the retinal cofactor attached to the seventh transmembrane helix. B) The all-*trans* retinal isomerising into 13-*cis* retinal upon light stimulation of microbial rhodopsins. C) The most known microbial rhodopsins: Halorhodopsin, Bacteriorhodopsin (bR), Channelrhodopsin-2 (ChR2), Sensory Rhodopsin II (SRII) in complex with its transducer HtrII (SRII:HtrII) [18].

While the 7TMs are consistent across all microbial rhodopsins, variations in the sequence and structure, as well as the number of conserved side chains, the orientation of loops, and the position of water molecules can be observed.

1.4 Sensory Rhodopsin in isolation and in complex with its transducer

1.4.1 Origin

Sensory Rhodopsin I and II (SRI and SRII) are microbial rhodopsins initially identified in *Halobacterium salinarum*, a halophilic member of the archaea growing in high concentrations of sodium chloride near or at saturation. They are respectively positive and negative phototaxis sensors regulating the direction of the cell movement based on the light stimuli [20]. SRI has a positive phototaxis response to green/orange light while SRII has a negative phototaxis response to blue light [14]. SRII from *Natronomonas pharaonis* (NpSRII), an aerobic, haloalkaliphilic member of the archaea, has been extensively studied due to its high stability during purification and the possibility to express it in *E.coli* [21].

1.4.2 Function

SRI and SRII work in complex with the *Halobacterial integral membrane transducer proteins* HtrI and HtrII to control a pathway that regulates cell motility [22]. The pathway is called *Two-component signalling cascade* and it has gained attention because of the potential pharmaceutical implications due to its ubiquity among prokaryotes and some eukaryotes. This mechanism is able to regulate a response to cell division, metabolism, pathogenicity, antibiotic resistance, and photo- and chemo-taxis [23].

As illustrated in figure 1.4, in the two-component signalling cascade, light is sensed by SRI or SRII and triggers the isomerisation of the retinal from all-*trans* to 13-*cis* conformation. The isomerisation of the retinal induces conformational changes on SRI or SRII, and this consequently affects the transducer HtrI or HtrII leading to a phosphorylation-mediated movement of the flagellum [21]. Indeed, these conformational changes are sensed by HAMP domain that conveys the signal to the histidine kinase CheA, bound to CheW, its adapter protein. CheA autophosphorylates and transfers the phosphate either to CheY, which activates the flagellar motor, or to the methylesterase CheB that regulates the feedback response together with the methyltransferase CheR [24]. When the bacterium needs

bacteriorhodopsin (bR) to produce ATP to satisfy its energy requirements, SRI is activated and the bacterium moves towards illuminated areas. When enough ATP is produced, SRII will apply negative phototaxis and the bacterium will move towards darker areas.

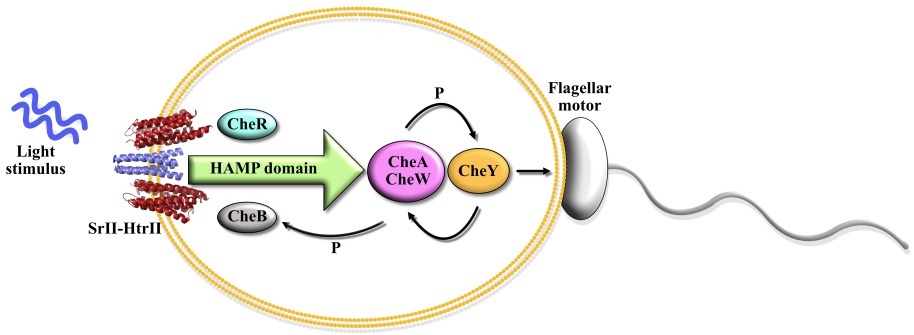

Figure 1.4: Two-component signalling. In the original organism *N.pharaonis*. The light stimulates the retinal isomerisation leading to SRII-HtrII conformational changes. These are perceived by the HAMP domain that transfers the signal to CheA and CheW. CheA autophosphorilates and transfers the phosphate either to CheY activating the flagellar motor, or to CheB and CheR for a feedback response. Image adapted from [24], [25].

1.4.3 Structure of SRII alone and in complex with its transducer HtrII

X-ray crystallography has been used to determine the structure of *Natronomonas pharaonis* SRII in isolation [26], [27], and in complex with HtrII [14], [24], [28], [29], showing high similarity to those of bacteriorhodopsin (bR) [26], [27]. Like all the microbial rhodopsin family members, SRII (Fig.1.5) is a seven helix transmembrane (A-G) protein with the retinal chromophore covalently attached to the conserved Lysine205 in helix G through a protonated Schiff base [21]. The transducer was believed to be located adjacent to helices F and G and the interaction was confirmed when the crystal structure of the SRII:HtrII complex was solved [24], [28], [29]. This X-ray structure revealed the transducer protein as two additional helices bound laterally in the membrane with the transmembrane helix 2 (TM2) positioned between helices F and G of SRII

and the transmembrane helix 1 (TM1) diagonally opposite and tilted away from helix G.

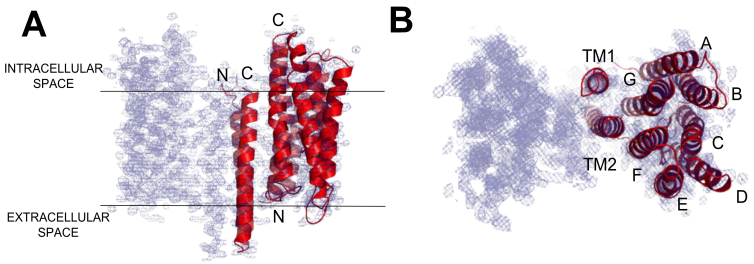

Figure 1.5: Structure of the complex SRII:HtrII (PDB ID 7ZCM). A) Front view showing the asymmetric unit. B) Top view with the helices labelled.

1.4.4 Photocycle of Sensory Rhodopsin II and comparison to Bacteriorhodopsin

SRII and bR are both model systems belonging the microbial rhodopsin family, extensively studied to understand the mechanisms of signal transduction and phototaxis. They both have the retinal cofactor bound to the conserved Lysine residue on helix G (Lys205 for SRII and Lys216 for bR). Light triggers the retinal isomerisation and the breakage of the salt bridge between the Schiff base nitrogen and its counterion (Asp75 in SRII and Asp86 in bR). As a result, a proton is transferred between the two [30] and a photocycle starts. In both SRII and bR there are similar intermediates called J, K, L, M, N, and O states (Fig.1.6) [25], [31]. The noticeable difference between these two proteins is the duration of the photocycle, lasting 2 seconds for SRII (due to a very long transition in the M-to-O state) and up to 10 milliseconds in bR. Another major difference is the proton transfer pathway. In bR the proton moves from the cytoplasm to the extracellular side, while SRII retains a proton from the extracellular side and releases it in the same side when deactivated [32]. These differences are presumably due to the different functions of the two proteins, with SRII being a photophobic sensor, and bR being a proton pump [33].

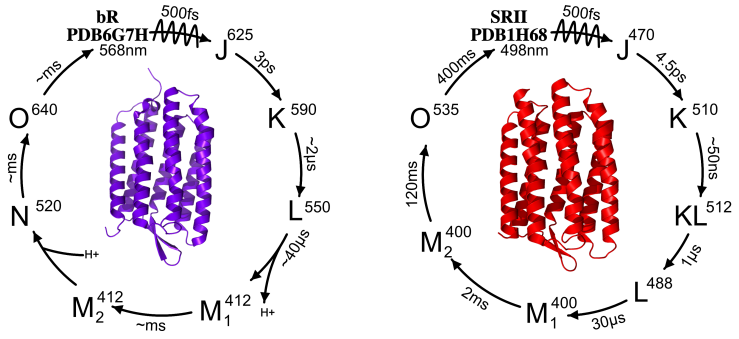

Figure 1.6: Left) Photocycle of Bacteriorhodopsin adapted from [34]. Right) Photocycle of SRII adapted from Bosman et al. (Paper I). In the figures, the spectroscopic intermediates with the corresponding wavelengths (in nanometers) and the time-frames in which the change occurs are shown.

1.4.5 Photocycle of SRII:HtrII

SRII alone and in complex with HtrII have small key differences in the photocycle, but they can be considered to be very similar (Fig.1.7).

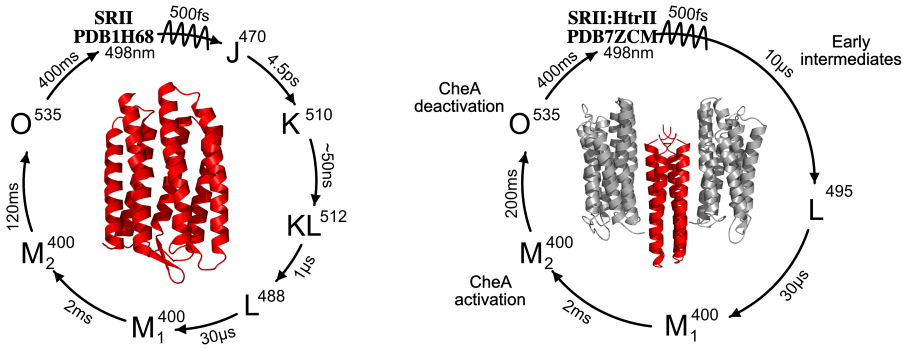

Figure 1.7: Left) Photocycle of SRII adapted from Bosman et al. (PaperI). Right) Photocycle of the complex SRII:HtrII adapted from [30]. In the figures, the spectroscopic intermediates with the corresponding wavelengths (in nanometers) and the time-frames in which the change occurs are shown.

The helix motions in SRII alone and in the SRII:HtrII complex differ in the extent of their movements upon activation, which are more pronounced in the absence of the transducer [35] (**Paper IV**). The proton transfer between the Schiff base and Asp75 defines the passage into M1 conformation. In M1-M2 transition Helix F of SRII gets close to TM2 triggering the kinases activation that later gets deactivated in O conformation [25]. SrII:HtrII complex photocycle has a slower decay of the M intermediate compared to the SRII alone [36], [37].

1.5 Aim of the work

Microbial rhodopsins are light-activating membrane proteins present in all kingdoms of life. They regulate key physiological mechanisms essential for life and survival in many organisms and have gained a lot of interest in the scientific community thanks to their potential medical and pharmaceutical applications.

Here we focus on SRII alone, and in complex with HtrII. We want to observe the structural features in both the photoactive and ground state to better understand their function. We want to (i) analyse the SRII photocycle and understand why, despite structural similarities, it is slower than bR, (ii) observe the SRII:HtrII complex structural features using serial synchrotron X-ray crystallography (SSX) at room temperature and investigate if a an alternative method to cryo-trapping leads to new structural information, (iii) study the light-activated SRII:HtrII with serial synchrotron X-ray crystallography (SSX) and characterise the transduction of the signal in the complex, and (iv) to observe the overall movement of the SRII alone and in complex using X-ray solution scattering (TR-XSS) to assess if the extent of the helical displacement in SRII alone or with HtrII have the same extension.

Chapter 2

Methods

Structural biology studies the structure of molecules like proteins and nucleic acids, both in their resting state and also aims to characterize their conformational dynamics. This implies the necessity of a multidisciplinary approach, involving biology, chemistry, and physics. In particular, when it comes to protein crystallography, it requires a molecular biology approach in the first phases of the study, with the protein identification and insertion into the right vector, its production, and its expression.

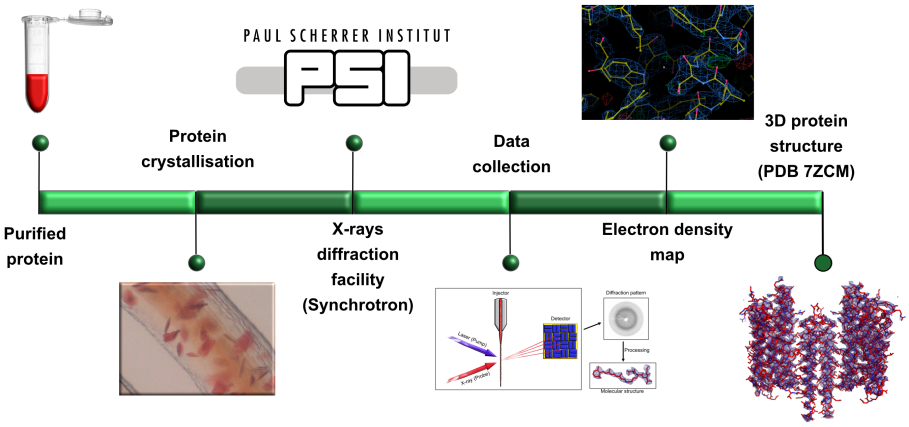

Figure 2.1: Workflow from the purified protein to a 3D structure.

Then biochemistry is involved when it comes to its purification, chemical physics for its crystallisation, and physics for the data collection, and a mix of them for the data analysis. In figure 2.1, the workflow from an

already purified protein sample to the creation of a 3D protein structure is represented. After protein purification, protein crystals are made and and sent to a synchrotron or an X-FEL facility where diffraction data are collected. If the quality of the crystals diffraction has a good resolution, an electron density map is generated. The collected data will be indexed, scaled and merged, and refined until a good 3D structure of the protein of interest is obtained. Here we explain the workflow outlined above, starting from the cell production.

2.1 Cell production and protein expression

The availability of a large amount of sample is essential for the success of protein studies. In the past, scientists required large quantities of original tissues or fluids to extract proteins from, and this was a big limitation in terms of quantity of available protein. Thanks to the advances of protein engineering, this limitation has been overcome by the use of recombinant proteins expressed in cell cultures [38].

Recombinant proteins are proteins transcribed and translated from a DNA sequence belonging to an exogenous organism that has been inserted into a host organism. Nowadays it is possible to express recombinant proteins using both prokaryotic (e.g. *E.coli* for SRII and HtrII) and eukaryotic (e.g. *P.pastoris* for ChR2) systems. The choice of the plasmid, the most suitable host cell, and the expression strategies, requires an optimisation that varies in each case [38]. This is highly affected by the characteristics of the protein, the post-translational modifications that may interfere with the crystal formation, the ease in which cells can be manipulated, the cell growth rate, and the yield of expressed protein [39].

To be able to produce and express a protein outside of its original organism, the DNA sequence with the genes encoding for the protein of interest needs to be cloned, and then inserted in an expression vector (e.g. a plasmid). In the case of bacterial and yeast cells, the plasmid carries both the genes expressing the protein of interest and the genes for antibiotic resistance like Kanamycin for *E.coli* or Zeocin for *P.pastoris*. This needs to be transformed into the new host. Once the transformation is done, the cells will be grown in a medium where specific antibiotics are present.

If the transformation has been successful, only those cells expressing the protein and the antibiotic resistance genes will grow. From this culture, single colonies will be selected and grown on a large scale. Paying attention to temperature, pH, and solutes in the growth medium is essential, and the type and concentration of the protein expression inducer (e.g. IPTG for *E.coli* and methanol for *P.pastoris*) should be carefully chosen [40], [41]. Once the protein is expressed, this can be purified from the host organism and further studies can be made [41].

2.2 Protein purification

2.2.1 Lysis of membrane

The lysis of the cell is the disruption of its cellular membrane. In structural biology, this is a common process to purify and study the cell membrane components or the intracellular material (e.g. nucleic acids, proteins, organelles). This is the first step of the separation and purification process and the most suitable method is selected based on the target intended to study. The lysis main goals are the efficiency of the disruptive process, as well as the maintenance of the target functionality [42].

Prokaryotic and eukaryotic cells have substantial differences in their membrane composition. Prokaryotic cells are smaller and simpler cells and they encompass all bacteria and archaea like *E.coli*. In general, they have a plasma membrane and an outer cell wall composed of peptidoglycans that can make thicker layers in gram-positive bacteria, or thinner layers in gram-negative bacteria [43]. Eukaryotic cells are found in yeasts, animals, plants, and fungi. In eukaryotes, the cell membrane consists of a phospholipid double layer where proteins are tightly attached and integrated into it.

The lysis of the cell membrane can be done both by mechanical and non mechanical methods. Mechanical methods are high pressure homogenisation by french press or homogeniser, and mechanical disruption by the beads beater where glass, ceramic, or steel beads have the disruptive function. Non mechanical methods can be divided into physical (freezing and thawing, sonication, osmotic shock), chemical (detergents and alkaline substances), or biological (enzymes) [43], [44]. During our research, the most suitable lysis methods have been the mechanical ones

and we will focus more on them. Mechanical methods use sheer force to damage the cell membrane and break it.

High-pressure liquid homogenisation

High-pressure homogenizers are devices that disrupt cells by introducing them in a small chamber through a narrow gap using pressure [42]. Sometimes the cells are also directed towards a surface at a very high speed, inducing an additional cell breaking. When the pressure is constant, the temperature can increase, so it is important to use a cooling system and protease inhibitors to avoid protein degradation. To increase the efficiency of lysation, this process may require to be repeated 2 or 3 times. This technique is very efficient for disrupting bacterial cells like *E.coli* although, despite a lower efficiency, it can be used also for eukaryotic cells. This method is useful for big volumes of samples.

Mechanical disruption with glass beads

The bead beater method consists of disrupting the cell membranes using the mechanical force applied by glass beads against cells during agitation promoted by a mixing mill. It is a very suitable strategy to break eukaryotic cells like *P.pastoris*. The size of the cell, the density of the cells, the beads size, and the agitation force are critical variables in this process. Keeping the temperature low and using protease inhibitors is essential to avoid protein degradation.

2.2.2 Cell membrane separation and solubilisation

Once the cell membrane has been disrupted, a series of centrifugation steps are done to separate the cellular membrane from the cytoplasm content. Then, if the focus of the study is on membrane proteins, the cell membranes should be solubilised and the membrane proteins isolated.

The solubilisation of the cell membrane is a process where the membrane proteins are extracted from their original environment into an aqueous environment usually by the use of the appropriate detergents. This is a very critical step because it may lead to the loss of function of the protein.

Detergents are amphipathic substances with hydrophilic heads and hydrophobic tails used to solubilise the cell membranes by mimicking the phospholipid bilayer. The most used detergents in crystallography are n-dodecyl-β-d-maltoside, n-decyl-β-d-maltoside, and n-octyl-β-d-glucoside [45]. They disrupt the phospholipid bilayer by saturating the bilayer that consequently breaks apart, and enclosing membrane lipids and proteins into micelles as shown in figure 2.2.

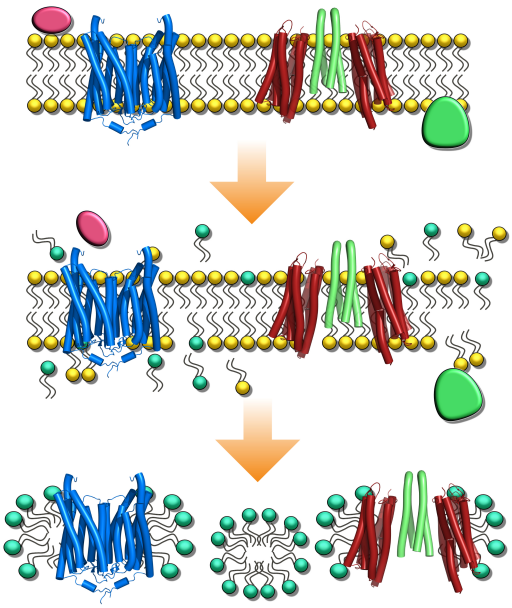

Figure 2.2: Membrane solubilisation and micelle formation. The integral transmembrane proteins ChR2 and the complex SRII-HtrII are respectively in blue and green-red. In pink is the peripheral membrane protein and in green the integral membrane protein. The phospholipids composing the cellular membrane are shown with yellow heads while the detergent has emerald green heads. The insertion of the detergent in the buffer disrupts the cellular membrane and incorporates membrane proteins inside micelles.

Inside the micelles, the membrane proteins have their hydrophobic surfaces facing the lipid tails of the detergent while the hydrophilic part is

in contact with the aqueous environment [45]. The solubilisation of *E.coli* membranes based on the SRII:HtrII purification protocol required an initial centrifugation at 15000 x g for 20 min followed by ultracentrifuge to sediment membranes (45TI, 43500 rpm or 70TI, 45000 rpm, 60 min) followed by homogenisation and resuspension in buffer with 5% n-octyl-β-d-glucoside overnight.

2.2.3 Chromatography

Chromatography is a biophysical method used to separate a mixture of proteins in a solution. These can be separated based on their size, shape, charge, presence of hydrophobic groups on their surface, or affinity with the stationary phase. There are four separation methods and they are based on the molecular characteristics of the solution. The most common methods are ion exchange, surface adsorption, partition, and size exclusion chromatography [46].

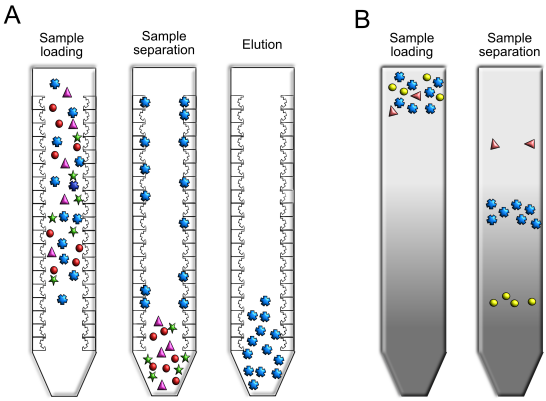

Figure 2.3: A) Affinity chromatography. B) Size exclusion chromatography.

In general, there are a stationary phase (liquid or solid) and a mobile (liquid or gas) phase. The solution containing the protein mixture is moved along the stationary phase by the mobile phase. Many chromatography methods can be used, but I will explain the two that have mostly been used to study SRII-HtrII complex.

Affinity chromatography

The aim of this method shown in figure 2.3 A, is to separate the target protein from a protein mixture based on its affinity to the binding partners in the stationary phase. The stationary phase, having a high affinity for a specific ligand (e.g. His-tag in case of NiNTA resins), is equilibrated and inserted in the column. Then, the mobile phase consisting of the protein mixture in solution will be introduced and will flow through the stationary phase. In the mixture, the target protein has a specific peptide or protein sequence showing high affinity for the stationary phase (e.g. 6-14 Histidine residues), so, this will bind to it, while the others will flow through. Then a few washes with an increasing concentration of imidazole will be done to remove all the unspecific or weakly binding proteins. Once everything unwanted has passed through, an elution buffer with the highest concentration of imidazole is used to disrupt the interactions between the stationary phase and the bound proteins. The protein of interest at this point will flow through and will be collected for further purification steps [47].

Size exclusion gel chromatography

Gel filtration chromatography (Fig. 2.3B), is a fractionation method that separates a protein mixture based on its size. The stationary phase consists of a porous substance with different pore sizes that have no interaction with the mobile phase. Once the mobile phase with the previously filtered protein mixture is applied to the column, the sample will elute at different times depending on the size of its components. The larger proteins will flow through faster than the smaller ones because the latter will be trapped in the pores, and they will all be collected in fractions at the end of the column. In general, proteins of the same size will flow through the column at the same time. This allows the user to fractionate the sample based on the size [48] and to separate the fraction containing the protein of interest from the rest in a very high level of purity.

2.3 Protein crystallisation

Protein crystallisation is a process where purified proteins in a homogeneous highly concentrated solution [49] are ordered in a repetitive, closely packed, three-dimensional crystal structure.

2.3.1 What is a crystal?

A crystal is a regular array of repetitive units arranged in a three-dimensional space in an ordered manner. Crystals have symmetrical properties and diffraction properties. The smallest repeating unit within a crystal is called the *unit cell* and it is described by three vectors *a, b*, and *c*, that indicate the length of the unit cell in each dimension, and three cell angles called α, β and γ located to the opposite side of each vector. The unit cell repeats itself by translation along with the crystal in three dimensions and sets the limits for the crystal lattice. The *crystal lattice* is defined as a regular array of points repeated *ad infinitum*. Once the unit cell is identified, this is associated with a *space group*. A crystallographic *space group* describes the symmetry of the crystal and all the combinations in which atoms can be distributed in space inside the unit cell. There are 230 space groups and they are subdivided in triclinic, monoclinic, orthorhombic, tetragonal, trigonal, hexagonal, or cubic [50]. Their nomenclature consists of a capital letter representing the lattice kind and a number describing the combination of symmetries within the unit cell. The *asymmetric unit* of a space group is a region of space, either a fraction of the unit cell or the entire unit cell if there is no additional symmetry, that not only is affected by translation but also by rotation, screw, reflection, and glide operations. It contains all the information describing the whole crystal [51].

2.3.2 Crystallisation techniques

Producing protein crystals is a challenging, time-consuming, and prone-to-failure process. Many factors like pH, temperature, ionic strength in the crystallisation solution, even gravity [52], and many other variables that cannot be controlled, influence the success of the crystallisation process.

If the challenge is accepted and time and patience are endless, many techniques can be applied. The two most common crystallisation techniques are *vapour diffusion* and *batch crystallisation*.
As presented in figure 2.4, the *vapour diffusion* method consists of mixing in a crystallisation drop both the concentrated protein solution and the appropriate precipitant solution, and enclosing them in a sealed chamber where the crystallisation buffer is present. The pressure of water vapour will increase and vapours will circulate between the drop and the crystallisation buffer until the same osmolarity values are reached between the two. During this process, the drop will slowly dehydrate until the protein will reach supersaturation and the nucleation process will start [53].

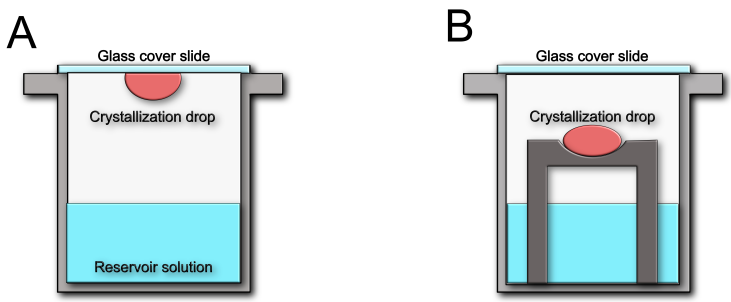

Figure 2.4: Vapour diffusion crystallisation techniques. In A the Hanging drop technique and in B the sitting drop technique.

There are two main vapour diffusion techniques: *hanging drop* and *sitting drop*. In the *hanging drop*, the protein/precipitant drop is hanging from a glass slide placed on top of the well containing the crystallisation buffer, while in the *sitting drop*, the mixture is positioned on a well above the crystallisation solution [54]. In *batch crystallisation*, the protein is placed in a well in direct contact with the right amount of precipitating agent and crystallisation buffer [53]. Before these methods can be used to crystallise, an initial screening to find the most promising condition is done using these methods on a smaller scale. During crystallisation it is fundamental to keep under control pH, temperature, precipitant concentration, and concentration of every additive present in the crystallisation buffer.

2.3.3 Lipid cubic phase in membrane proteins

The Lipid Cubic Phase (LCP) or *in meso* approach, is a well known strategy to crystallise integral membrane proteins. The solubilisation process and the use of detergents during the protein purification may disrupt the protein native conformation and often leads to the protein loss of function. This method is used to counteract this problem by restoring the protein native tridimensional conformation and consequently its activity [55]. This technique consists of adding phospholipids to the purified integral membrane protein solution to mimic the protein native environment. The most commonly used phospholipid is the monoacylglycerol monoolein (MAG), and it is used to form a mesophase consisting of MAG and water [56]. The method is executed by mixing the pure concentrated protein and monoolein with a proportion of 40% of the protein and 60% of the lipid. These two are initially inserted separately into two glass Hamilton syringes connected by a coupler and then they are mixed together by an alternate pressure of the plunger of the syringes [57]. Once the cubic phase is constituted, a batch crystallisation approach can be attempted and the LCP-protein mix is extruded from the syringe and put in contact with the crystallisation buffers in a crystallisation plate. The transformation from a cubic phase to a lamellar phase will cause the protein to concentrate. This, with the use of specifically selected crystallisation buffers, will hopefully lead to the nucleation phase, and crystal formation [56], [58].

2.3.4 Crystal formation

Growing good diffracting crystals is essential for the determination of a high resolution structure. To produce protein crystals, the sample needs to be close to homogeneity with a purity of at least 95% and have a concentration that can vary between 2 and 50 mg/ml. To crystallise membrane proteins, the purified protein solution should also be mixed with a phospholipid to form the LCP. Then, to crystallise, one of the previously explained techniques is executed [59].

Crystal formation occurs in two main steps: nucleation and crystal growth. As described in figure 2.5 by the phase diagram: nucleation is a phase where proteins in a supersaturated solution (the quantity of protein

exceeds the solubility limit) [60] engage a dynamic process where they randomly aggregate into a nucleus and go back into the solution.

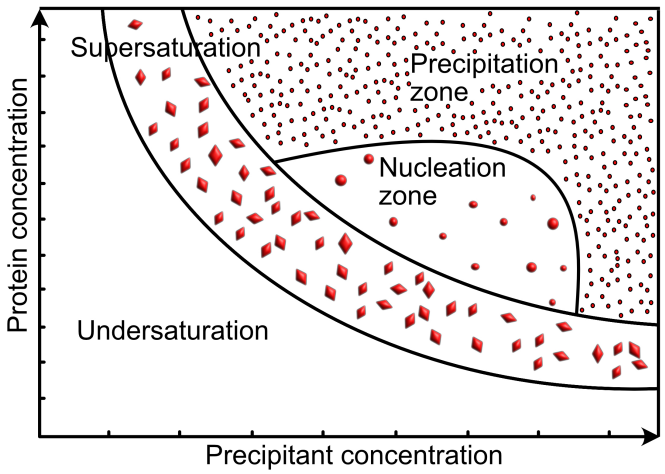

Figure 2.5: Crystals phase diagram adapted from [61]

This goes on until a sufficient size is reached to become a stable site of nucleation for the crystal formation [62]. If the both protein and the precipitant concentration are optimal, the protein undergoes the labile state and crystals will grow. The growth phase is a dynamic process in which more molecules will continue to aggregate around the nucleation point. This will cause a drop of the concentration of the protein in the solution. If the protein concentration and the amount of precipitant are not sufficient, the solution is undersaturated and the crystals will not form. If the concentration of protein and precipitant is too high, the protein precipitates but the formation of crystals may still occur [49], [54].

Depending on the purpose of the data collection and the chosen technique, the production of either a few big crystals or many small crystals may be preferred. This may be achieved by choosing the most appropriate crystallisation method and varying the concentrations of the crystallisation buffers and of the protein.

2.4 Theory of light scattering and X-ray diffraction

2.4.1 Electromagnetic radiation

Electromagnetic radiation (EM) is composed of electromagnetic waves. As described by Maxwell, electromagnetic waves originate from the interaction of two vectors perpendicular to each other respectively representing the electric and the magnetic field. The EM radiation can be described based on its wavelength and frequency. The wavelength is the distance between two peaks and is usually given in nanometers, while the frequency is the number of waves crossing a specific point every second and is expressed in Hertz (1/s). The wavelength and the frequency of EM radiation are described by the equation

$$c = \lambda\nu \tag{2.1}$$

where c is the speed of light that is a constant with a value of 3.8 x 10^8 m/sec, λ is the wavelength, and ν is the frequency. The electromagnetic radiation behaves both as a wave and a particle without mass. This particle is called a photon, and is described by the equation:

$$E = h \cdot \nu \tag{2.2}$$

where the photon energy E is described by h representing the Planck constant $6.626 \times 10^{-34} m^2 kg/s$ and ν its frequency. The spectrum of wavelengths of the electromagnetic field ranges from 10^{-15} m to 10^7 m [63]. As represented in figure 2.6, electromagnetic waves are grouped into radio waves, microwaves, infrared radiation, visible light, ultraviolet radiation, X-rays and gamma rays depending on its energy. Just a small part of the electromagnetic spectrum is visible to the human eye and this part ranges between 450 and 700 nm [63]. In the range of the visible light, the colours are the resulting wavelengths that are transmitted, reflected, scattered, or emitted by matter. The red colour corresponds to an EM radiation of λ about 700 nm, the violet about 430 nm, 500-550 is green, 550-600 is yellow.

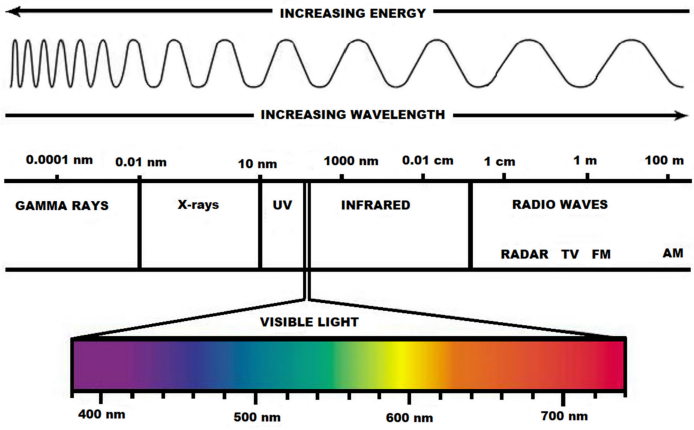

Figure 2.6: Electromagnetic spectrum [64].

Many living beings among bacteria, plants and animals evolved mechanisms enabling them to use a part of the electromagnetic spectrum for their vital functions. The most used is the visible light and examples can range from phototrophy to phototaxis to animal vision.

2.4.2 What X-rays are, and how they are generated

X-rays are part of the electromagnetic spectrum. The wavelength of X-rays range from 10^{-12}m to 10^{-9}m as shown in figure 2.6. They are subdivided into soft X-rays, X-rays, and hard X-rays depending on their energy. Hard X-rays are usually adopted in medical applications due to their ability to penetrate objects, and are those commonly used in X-ray crystallography. X-ray crystallography is a technique to characterise the structure of a molecule or complex organised in a crystalline structure, up to atomic resolution. X-rays are optimal for the purpose, because their wavelengths, ranging between 0.1 and 1 Å, have dimensions comparable to the interatomic spaces within the molecule of interest.

Synchrotrons

A synchrotron is a particle accelerator with a circular shape where electrons are accelerated to relativistic energies to produce an electromagnetic

radiation in the X-ray wavelength by using a magnetic field. Its structure is composed by a LINAC, a booster synchrotron, a storage ring, and beamlines. In the LINAC, electrons are accelerated to be injected in the booster. The booster is the part where electrons are accelerated from 1 to 8 GeV and it is active just few minutes a day to accelerate electrons and refill the storage ring. The storage ring is a tube where electrons travel close to the speed of light and the electron energies are kept constant. Inside the storage rings there are straight and curved sections. In the straight sections there are undulators with lengths up to 5m where X-rays are produced by the electrons forced into a sinusoidal trajectory. In the curved sections of the storage ring, there are bending magnets to bend electrons into a round shaped orbit. When the electrons are bent and change direction, synchrotron radiation is produced and energy lost [65]. To conclude, the beamlines are branches departing from the storage ring that possess specific setups adapted to the various research purposes. In my thesis, data in **Paper I**, **Paper II**, and **Paper III**, and **Paper IV** were collected at synchrotrons.

X-FELs

X-FELs are facilities with a linear shape used in protein structural biology to get information on ultrafast protein conformational changes in the order of femtoseconds. They have a higher peak brilliance and shorter pulses compared to synchrotrons. The advantage of using an X-FEL instead of a synchrotron relies on the dimension of the microcrystals that can be smaller, less radiation damage [66], the shorter time-frames in which data can be collected [67], and the resolution can be higher. They have a linear shape and are usually up to a few kilometers in length. Once electrons are accelerated, they will be forced into periodic array of magnetic dipoles called undulators where the electron trajectory will become sinusoidal causing the electrons to emit electromagnetic waves similar to the synchrotron radiation. The light is generated thanks to a phenomenon called Self Amplified Spontaneous Emission (SASE), where electrons interact with their emitted electromagnetic waves and the ones emitted by the adjacent ones. This process causes electrons to cluster together into short, powerful pulses of energy that can be many orders of magnitude

more powerful than synchrotron radiation [68]. In my work, data in Paper VI, Paper VII, and Paper VIII, data were collected in X-FELs.

2.4.3 Atomic and crystallographic scattering

When an incident X-ray beam, formed by parallel waves of equal intensity and phase encounters matter, this will be scattered by its electrons in different angles and phases (Fig.2.7). Based on how the X-rays get scattered, we can refer to elastic or inelastic scattering, or either to coherent or incoherent scattering depending on the phase of the waves. These interactions can lead to events like refraction, absorption, fluorescence, diffraction and many others.

Bragg´s law

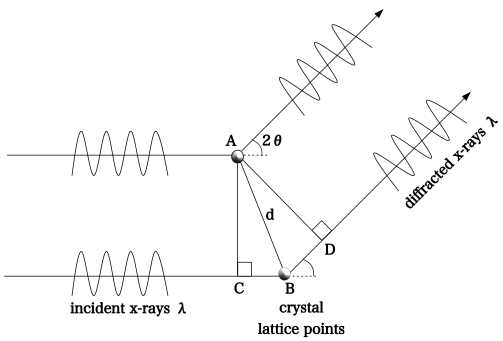

Figure 2.7: Atomic scattering. A and B are crystal lattice points, d is the distance between lattice points, θ is the angle formed by the scattered wave, CB=dsinθ, BD=dsinθ, CB+BD= 2d sinθ, λ is the wavelenght of the radiation, nλ = 2d sinθ.

If we consider two parallel planes with a distance d, (Fig.2.7) the difference path Δ between the two incident rays is equal to

$$\Delta = 2dsin\theta \tag{2.3}$$

where θ is the incidence angle. Bragg´s law (Eq.2.4) affirms that here is constructive interference between the two diffracted rays when

$$n\lambda = 2dsin\theta \tag{2.4}$$

where n is an integer, λ is the X-ray wavelength, d is the distance between two lattice points and θ is the angle formed by the scattered half deflection angle (Fig.2.7).
When there is costructive interference, meaning that the waves are scattered in phase, Bragg´s equation can be applied.

Ewald´s sphere

Bragg´s law can be geometrically interpreted in the reciprocal space with the Ewald sphere (Fig.2.8).

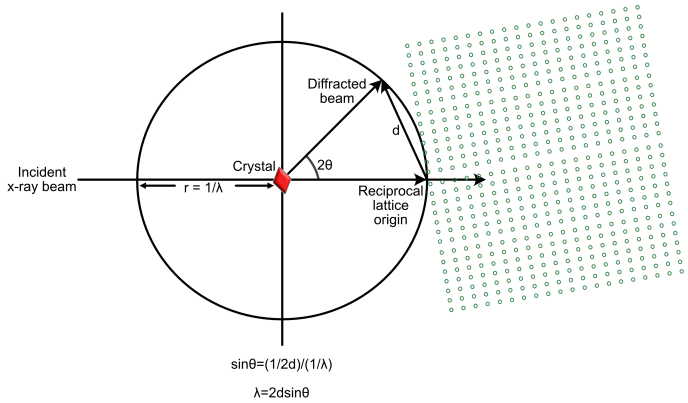

Figure 2.8: Ewald´s sphere, d is the change in X-ray scattering vector, 2θ is the angle formed by the scattered wave, λ is the wavelenght of the incident radiation, the ray of the sphere corresponds to $1/\lambda$, $sin\theta = (1/2d)/(1/\lambda)$, and n$\lambda$ = 2d sinθ.

When X-rays are scattered by a crystalline structure, the scattering will show waves heading towards many directions, and will be characterised by different phases and intensities. The intensity varies based on the contribution of the single waves, increasing with the increase of the number

of the scattered waves in phase travelling in the same direction, and decreasing when the waves are not in phase. When the scattered waves are from an array of identical repetitive units, this will define a diffraction pattern, that through Fourier transform, will give information about the crystal structure.

The Ewald sphere (Fig.2.8) is a sphere whose radius is the reciprocal of the wavelength of the incident X-ray beam $1/\lambda$. In the center of the sphere a crystal is positioned, and it sets the origin of the scattered vectors. The angle formed between the incident and scattered vector is 2θ, d represents the change in X-ray scattering vector. The intensity within the diffraction spots contains information on the crystal lattice, its symmetry and dimensions, and the atomic positions within the crystal.
Once data are collected, thanks to Fourier transformations, it is possible to visualise the structure of the molecule.

2.4.4 Cryo-crystallography

Cryo-crystallograpy is a static technique that averages in time and space the multiple conformations of the proteins present in a big single crystal [69]. With this method, data are collected at cryogenic temperatures to reduce the occurrence of radiation damage [66]. Cryoprotectants are used to preserve the lattice structure that may be disrupted by the presence of ice, and to avoid the presence of ice rings in the diffraction pattern. Due to a rigid glass-like structure, protein motion cannot be observed, but despite that, it has the advantage of better signal-to-noise ratio even for weaker diffraction compared to other methods. A typical cryo-crystallography setup consists of a steam of liquid nitrogen and a stream of dry air, both blowing towards the sample, to keep the temperature of the sample constant and prevent both radiation damage and ice formation. There are also a magnetic nozzle with a loop at the end of a robotic arm where the sample is placed, a goniometer to collect data on different angles, an X-ray beam pointing towards the sample, and a detector. The data collection process in cryo-crystallography nowadays is automated and it can be done remotely [70].

2.4.5 Time-resolved serial synchrotron X-ray crystallography (TR-SSX)

Time-resolved serial synchrotron X-ray crystallography (TR-SSX) is a new technique where data are collected using a continuous flow of microcrystals randomly oriented in space. This method can be executed both in synchrotrons and X-FELs, depending on the time-frame in which the chemical process of interest occurs. This is an approach that can be used to study protein dynamics [71]. In fact, compared to the traditional cryo-crystallography, time becomes a new variable in the data collection [72]. A conformational change is determined by the switch of the protein conformation between two or more energetically favourable conformations. This can be triggered for example by pH change or light activation.

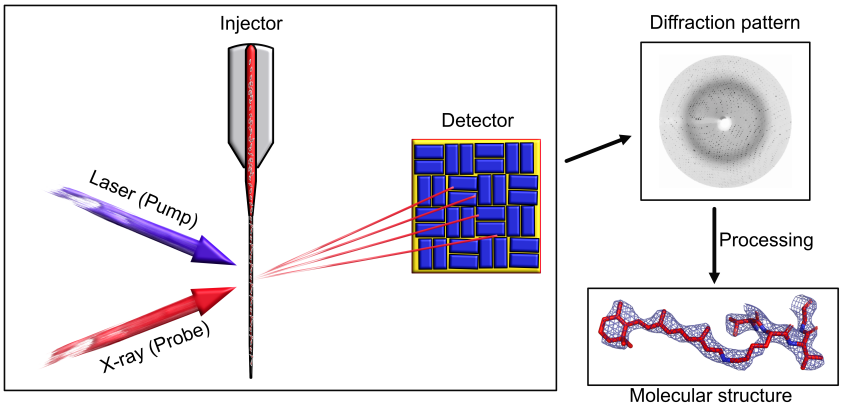

Figure 2.9: Time-resolved serial synchrotron X-ray crystallography (TR-SSX) setup and workflow, modified from [73].

In time-resolved crystallography, data are collected in room temperature, and to avoid sample damaging due to radiation damage, crystals are continuously replaced [74]. For the continuous replacement of crystals, injectors [75], fixed target [76], or continuous circulating tape are used [72]. The collection at room temperature also implies that the microcrystals are not as constrained by a glass-like structure as in cryo-crystallography, and upon photoactivation, the microcrystallised proteins

can move. For studies on light-driven systems, time-resolved crystallography uses the pump-probe approach to collect data (Fig.3.1). The pump is a laser at specific wavelengths in the visible spectrum that triggers reactions in light-sensitive proteins, activating 10-40% of them. A controlled time delay, the probe, an X-ray pulse, is used to collect the data at specific time intervals [69], [77]. TR-SSX setup for a pump-probe data collection, is shown in figure 2.9. A laser pump illuminates and initiates the photoreaction in the sample, and after a specific time-interval an incident X-ray beam hits the sample flowing from the injector. Part of the X-ray beam will be diffracted and sensed by the detector, where Bragg peaks will appear. In time-resolved datasets (**Paper I and IV**), a dataset with the non activated protein and a dataset with the activated protein are collected, the difference Fourier electron density map calculated, and a model is used to refine the structure against the experimental data.

2.4.6 Data processing and refinement

Data processing and refinement is a long process consisting of many different steps. The first step is the spot indexing, where the diffraction pattern (the intensity of the pixels) is correlated to Miller indices to assess the crystal lattice orientation. Then data are reduced. This means that many geometric parameters like detector position and distance, the radiation wavelength, the beam centre position, are assessed and introduced in the algorithm. Then the intensity of the diffraction spot is calculated (a threshold in the pixel intensity is set to discriminate among real diffraction and background) for background correction, and the unit cell parameters are given, to better assess the indexing of the peaks, and to minimise the difference between observed and calculated spots. Then the integrated intensities are scaled and merged. In the scaling, correction factors to minimise crystal volume variation, difference in X-rays absorption, and X-ray radiation damage are introduced, to make all the diffraction data comparable, while in the merging, equivalent observations are summed together [78], [79]. In particular, in the French-Wilson scaling, the merged intensities are corrected and made positive as they should be, and assumed to follow a Wilson distribution. After the scaling and merging process, some figures of merit can be calculated to assess the quality of

the dataset. Some figures of merit are: completeness, signal-to-noise ratio (I/σ), redundancy and R_{split}. The completeness describes the percentage of the reflections observed in each resolution shell, and its value should be close to 100%. The (I/σ) indicates how much stronger the diffraction is compared to the background. The redundancy indicates the number of reflections measured, and R_{split} is the agreement between two halves of the dataset.

The next step is the phasing, that is a complex issue to assess, often causing difficulties in interpreting data. Each diffraction spot represents a scattered wave from the h,k,l planes. Each wave is described by an amplitude and a phase. The amplitude of the wave F_{hkl} is proportional to the square root of the intensity. Amplitudes can be measured but the phases are lost in the experiment. To calculate the electron density in a specific position in the unit cell, a summation of all the hkl planes in that position needs to be performed.
In other words, the electron density ρ at a specific position (xyz) is the summation of all the scattered waves from the hkl planes in that point. The amplitude is given by the electrons in that plane and everything is corrected with the right phase relationship (Eq.2.5) [80].

$$\rho(xyz) = 1/V\Sigma_{hkl}F(hkl)^{[-2\pi i(hx+ky+lz)+i\alpha(hkl)]} \tag{2.5}$$

where V is the volume of the unit cell and αhkl is the phase associated with the structure-factor amplitude F_{hkl}. In my work we used molecular replacement to solve the phase problem, since the structure of SRII and SRII:HtrII had been previously solved. By applying the reverse Fourier transform to the structure factors, the electron density is obtained. When time-resolved data are collected from photoactive proteins, in order to highlight differences between the light-activated and the dark structures, we compute difference Fourier electron density maps:

$$(|F^{obs}|_{light}) - (|F^{obs}|_{dark}) \cdot exp[i\Phi_{calc}] \tag{2.6}$$

where the collected data from the inactive structure are subtracted from the light-illuminated data, and the phases are calculated from the refined dark structure. The difference Fourier electron density map (Fig.3.3) is

represented by positive difference electron density peaks in blue and negative in yellow. In the positive, there is the new electron density that arises in the active state and in the yellow there is the electron density that has been removed from the resting state [81]. Then a model is used and the data are refined in a iterative process until we get a final refined structure. We used this approach for studying the data collected from membrane protein crystals discussed in this thesis in **Paper I**, **Paper II**, and **Paper III**.

2.4.7 Time-resolved solution scattering (TR-XSS)

Time-resolved X-ray solution scattering (TR-XSS) is a method used to study global protein conformational changes over time. It allows us to study protein dynamics in solution and their conformational changes on timescales from femtoseconds to seconds, both for reversible and irreversible reactions.
TR-XSS does not require well-ordered crystals, but this comes at price as high resolution information is lost due to each protein molecule being randomly oriented. As such, TR-XSS can provide useful insights into secondary structure rearrangements but has the disadvantage that reconstructing the protein movements may not be unique [82]. Indeed, the scattering patterns are spherically averaged. A TR-XSS experiment in photosensitive proteins consists of triggering protein conformational changes in a protein in solution that flows through a quartz capillary connected to a motorized syringe pump with a laser pulse and then measuring the X-ray scattering with an X-ray pulse [77]. This pump-probe method consists of a laser (the pump) that photoexcites the protein of interest and after a specific time-delay, an X-ray pulse (the probe) probes the laser-illuminated volume of the sample [82]. The time-delays can be chosen based on the characteristics of the proteins and the speed at which the photocycle happens. Usually, logarithmic time-points are used to cover the dynamics over several order of magnitude.

The scattering curves are an ensemble of background due to the capillary, the scattering from buffer surrounding the protein, the scattering from the protein, and the heating of the sample. All of those effects need to be handled to isolate a difference signal from the protein. Data need

to be normalised and contribution other than the protein needs to be subtracted [69]. We used this method in **Paper IV**.

Chapter 3

Paper I

3.1 Structural basis for the prolonged photocycle of Sensory Rhodopsin II revealed by serial synchrotron crystallography

Microbial rhodopsins are a family of light-activated heptahelical transmembrane proteins characterised by the presence of a retinal chromophore which covalently binds to a Lysine residue on helix G through a protonated Schiff base (SB). Sensory Rhodopsin II and Bacteriorhodopsin (bR) are both members of the microbial rhodopsin family. They are model systems used to understand signal transduction and phototaxis. Upon photoactivation, the retinal isomerises from all-*trans* to 13-*cis* and transfers one proton to the proton acceptor Asp85 in bR, or Asp75 in SRII [83] during the L-to-M phase. Although similarities in the structure, these two proteins differ in the photocycle length, due to a longer M-to-O transition required by SRII for the signal transmission. This might be explained by the different functions of the proteins, where SRII is a phototactic sensor with photophobic reactions to blue light, while bR is a proton pump, creating a proton gradient to produce ATP [84].

Time-resolved serial synchrotron X-ray crystallography (TR-SSX) data have been collected at room temperature on Sensory Rhodopsin II at the Swiss Light Source (SLS) to better explain its prolonged photocycle. SRII data have been compared to previously published bR data collected in the same conditions [31], [85].

3.1.1 Room temperature SSX resting state structure of SRII

N.pharaonis SRII has been grown and expressed in *E.coli*. The purification process required the use of high concentrations of detergents to reach the purity level required for a high-resolution structure determination. We restored the protein native conformation through the use of phopsholipids that mimic the native protein environment. Previous purification protocols used purple polar lipids isolated from H. salinarum [9], [27], [35], [86], [87], but our attempt to replicate this method did not give us the outcome we hoped for. We instead succeeded to produce microcrystals with the LCP method where monoolein had 15% phytantriol added. Microcrystals took 1 to 2 months to grow. Serial crystallography data have been collected using microcrystals in LCP at the SLS. Data have been processed, scaled, and merged with Crystfel [88]. We used the phases from PDB entry 1H68 [27] for the molecular replacement, and Phenix [89] for the refinement. The light-activated structure underwent partial occupancy refinement, where 30% was light activated. The isomorphous difference Fourier electron density map $(|F^{obs}|_{light}) - (|F^{obs}|_{dark}) \cdot exp[i\Phi_{calc}]$ was calculated with Phenix using the phases from the dark structure. The resulting space-group is $C222_1$, with a the unit cell a= 89.8, b= 131.7, and c= 51.4, presented a resolution of 2.1 Å for the dark inactive structure of SRII, and 2.5 Å for the light-illuminated.

3.1.2 Photoactivation of SRII microcrystals within a LCP microjet

Light-activated and dark datasets have been collected interchangeably every 30 minutes. In the 30 minutes of light data collection, as shown in figure 3.1, the sample was illuminated for 5 milliseconds at 4Hz (pump) and the X-rays collected data for 250 milliseconds (probe). Data were initially grouped in 10 milliseconds bins, but successively the groups were expanded to about seven 30 ms bins, and one 40 ms bin, due to a slow photocycle of SRII. We presented the difference Fourier density of the structure in a one-dimensional map onto the protein sequence [90] to better understand the time-resolution of the helical displacements (Fig.3.2).

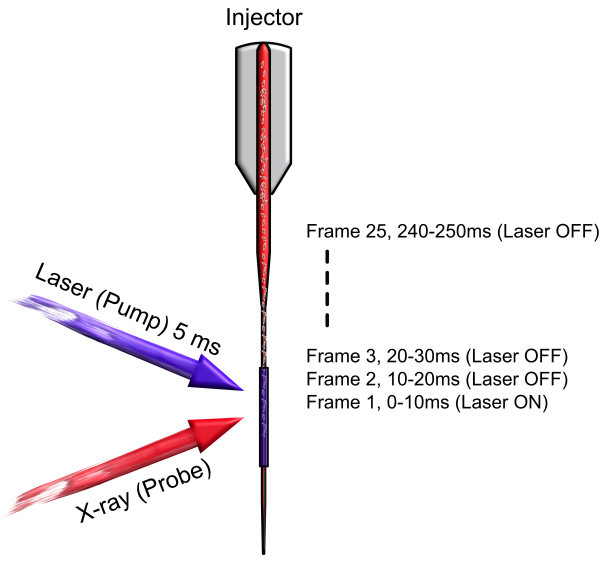

Figure 3.1: Pump-probe data collection. The sample is extruded by the injector in a continuous flow. The laser is activated for 5 milliseconds, then the sample is probed for 250 milliseconds.

Our analysis has shown that upon photoillumination, the illuminated part of the SRII sample was cleared in 120 ms from the X-rays. The following time-points did not present any helical displacement and they were considered unexposed. Relevant in figure 3.2 are the first two lines, where the helical displacements upon continuous illumination both for bR and SRII are shown, further confirming our observations.

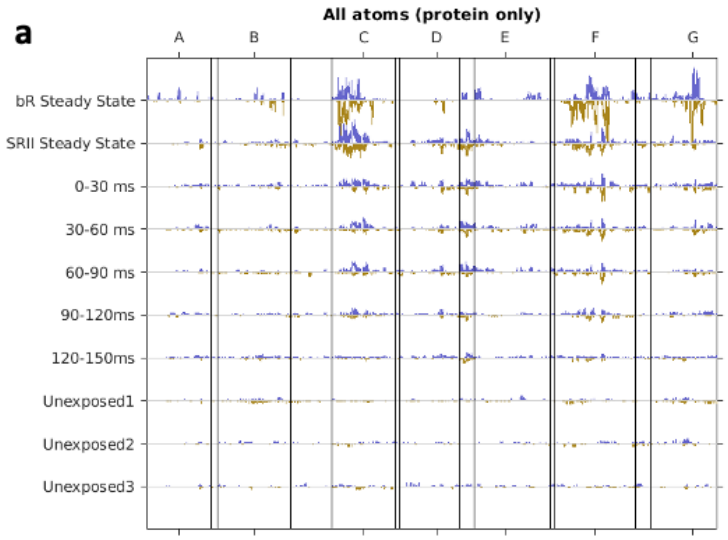

Figure 3.2: Time-dependence of difference electron density features in SRII. a) Difference electron density changes represented as a function of residue number according to the procedure described by Wickstrand et al. [90]. Similar difference density features are observed for bR and SRII during continuous illumination, and in the time-resolved data after a 5 ms laser-flash.

3.1.3 Light-induced rearrangements of extracellular water networks and helix C

We calculated a difference Fourier electron density map for both SRII and bR by subtracting the dark dataset to the photoilluminated one [31], and then we compared them. In the photoactive structure of SRII and bR we can observe water displacement, indicated by the negative electron density around the water molecules (Fig.3.3). Upon retinal isomerisation in bR, the hydrogen bond between the SB and a structural water molecule (Wat402) breaks. Water disorder is further confirmed by a strong negative electron density on Wat400, Wat401 and Wat402, and a positive density on Wat450. This disordering is essential for bR to trigger a cascade of conformational changes. The same happens with WatA2 in SRII, and this observation is consistent with the freeze-trapping studies on this protein

[9], [29], [91]. Furthermore, in SRII, a negative density around WatA5 and WatA19 and a positive electron density around WatB4 (not shown) indicate the transient ordering of a new water molecule. These water rearrangements are necessary for helix C to move towards helix G, involved in the proton exchanges both in SRII and in bR. Furthermore, as the SB is deprotonated in bR, the H-bond between Thr89 and Asp85 breaks. This is brought up by a negative electron density between these two residues, and with another negative density feature on Asp85, suggesting a movement that prevents the reprotonation of the SB.

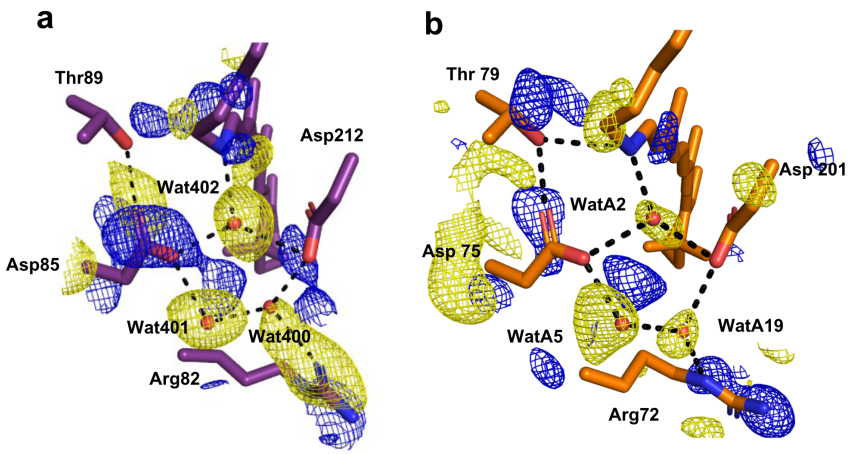

Figure 3.3: Difference Fourier electron density map showing waters disorder. a)bR. b)SRII. Blue represents positive difference electron density and yellow negative difference electron density. Both contoured at 3.0 σ, where σ is the root mean square electron density of the map.

This is essential for the function of bR as a proton pump. In contrast, in SRII the bond between Thr79 and Asp75 does not break, and coupled positive and negative densities suggest instead a movement of these residues towards each other. This is consistent with SRII not being a proton pump, so the bond does not need to be broken.

3.1.4 Light-induced movements of the extracellular portions of helices D, and E

The extracellular portion of helix C moves, and due to the tight packing with helices D and E, it causes the displacement of the extracellular portion of these two helices also moves. This displacement is observed in both SRII and bR, despite in SRII this is more extended (Fig.3.4), probably due to the association of helix D and E with the spectral tuning of this protein [92].

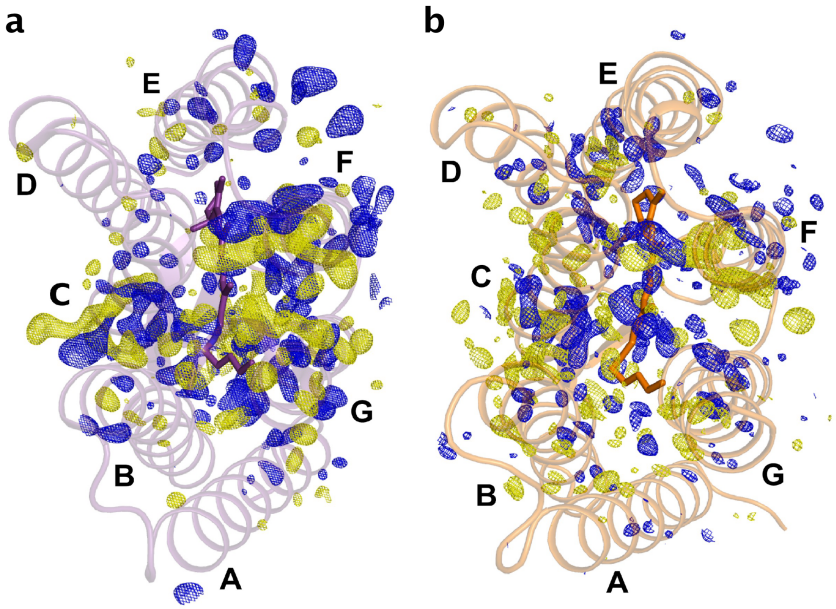

Figure 3.4: Difference Fourier electron density maps of bR and SRII from SMX datasets upon continuous illumination. a)bR. B)SRII. Blue represents positive difference electron density and yellow negative difference electron density.Both contoured at 3.0 σ, where σ is the root mean square electron density of the map.

Previous time-resolved studies suggested that the movement of helix C is the rate limiting step controlling the L-to-M transition [93].

3.1.5 Light-induced movements of helix F

Difference Fourier electron density maps of both SRII and bR present paired positive and negative difference electron density features on helix F (Fig.3.4), suggesting an outward movement of helix F cytoplasmic portion. This movement is more extended in bR, with a $C\alpha$ displacement of 3.78 Å, being measured in on TR-SSX study. By contrast, in SRII the movements in this region achieve an rmsd of 0.71 Å. When retinal isomerises, its C20 methyl group has steric clashes with Trp182 in bR and Trp171 in SRII, causing these residues to move towards the cytoplasm. This distancing causes an outward movement of helix F also observed by TR-SSX [31], TR-SFX [93], time-resolved X-ray solution scattering [94] and spin labelled EPR spectroscopy [95].

3.1.6 Light-induced rearrangements within helix G

In the resting state structure of both the proteins, H-bond water bridges between Trp171 and Thr204 in SRII, and with Trp182 and Ala215 in bR are located between helix F and G (Fig.3.5). In bR, the water-coordinated H-bond Trp182-Wat404-Ala215 is characterised by paired positive and negative difference electron density and it is believed to be involved in the unwinding of helix G. Indeed, the steric clash between C20 methyl group of the retinal and Trp182 pulls Lys216 on helix G, increasing the distance of helices F and G, and breaking the water bridge. The distancing of helices F and G in their cytoplasmic portion facilitates the reprotonation of the SB from Asp96 due to the H-bond breakage. Furthermore, the helix G displacement causes Lys216 to break the H-bond with Gly220 that becomes then available to bind waters. Wat404, Wat453 and Wat454 create a transient water-mediated H-bond between the SB and Asp96, helping the reprotonation of the SB. In SRII, despite a movement of helix F, the corresponding movement of helix G does not occur. This is due to the presence of water-mediated H-bonds (Trp171-WatA1-Thr204), H-bonds between Thr204 and Tyr174 on helix F, and H-bonds between Thr204 with Leu200 and Asp201 on helix G. Thr204 is a key residue preventing the helix G movement, and this was also confirmed by EPR and FTIR studies [37], [96]. The absence of movement on helix G in SRII

is believed to prolong the M-state, causing in SRII a longer photocycle compared to bR. In bR, a movement in helix G in concert with the retinal isomerisation is observed. This is due to the involvement of this movement in the reprotonation of the Schiff base(SB).

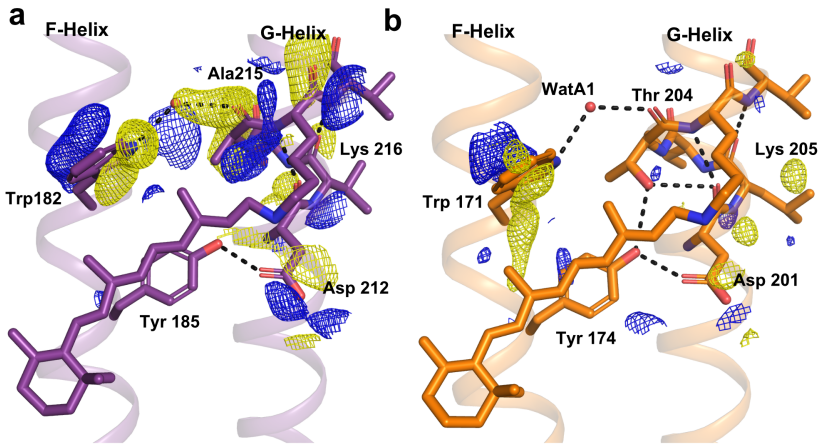

Figure 3.5: Structural changes of bR and SRII from the cytoplasmic side of the retinal upon continuous illumination. a)bR. B)SRII. Blue represents positive difference electron density and yellow negative difference electron density. Both difference Fourier electron density maps are contoured at 3.0 σ.

3.1.7 Conclusions

TR-SSX is a useful strategy to approach the study of protein movements through the observation of the electron density changes. This enabled us to understand structural fluctuations of our proteins, and gave us insights into how the movement of helix G and the key residue Thr204 influence the photocycle duration in SRII. Being able to retrieve this detailed, yet subtle, information about protein motion on this membrane protein hints at many future applications in the field of biochemistry.

Chapter 4

Paper II

4.1 Serial millisecond crystallography structure of the Sensory Rhodopsin II transducer complex.

Sensory Rhodopsin II is tightly bound in a complex with its transducer HtrII. Upon photoactivation, the retinal isomerises causing the initiation of a photocycle that gives rise to a cascade of signalling events called *Two-component signalling*, which leads to the negative phototaxis from blue light in its host organism *N.pharaonis*. Data from previously published structures collected at cryogenic temperatures have shown a structure with the transducer helices (TM1 and TM2) being bound to helix F and G of SRII, with TM1 diagonally opposite to helix G, and TM2 wedged between helix F and G [9], [24], [29], [97]. Here we present a 2.85 Å structure of the complex with a truncated transducer (residues 1-114) in its inactive state using serial synchrotron X-ray crystallography (SSX). The structure is consistent with previously published structures and shows five additional modelled residues on the cytoplasmic side of TM1 of HtrII.

4.1.1 New crystallisation conditions

A purification of SRII:HtrII complex was devoloped that does not involve anymore the resuspension in purple membrane lipids. The addition of phytantriol, having a similar phase diagram to monoolein, has been observed to aid crystallisation. Microcrystals of the complex were grown using the

batch method and they have been transported to SLS for data collection at room temperature using an LCP injector. The space-group of our SRII:HtrII is $P2_122$, the unit cell: a= 52.9, b= 67.7, c= 114.4, and the resolution 2.85 Å.

4.1.2 Machine learning improvements of the electron density map

Data have been indexed, scaled and merged using traditional methods [88], but the structure could only be solved at low resolution. We therefore decided to explore a new approach using Careless [79], a deep learning algorithm for scaling and merging using French-Wilson statistics [98].

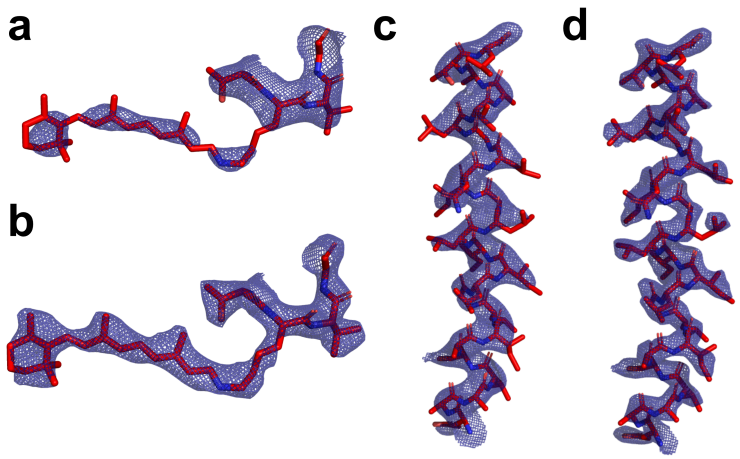

Figure 4.1: Improvement in the SSX electron density map of the complex using Careless algoritm. a) $2F_{obs} - F_{calc}$ electron density map (blue mesh) along the retinal chromophore and Lys205 when using traditional merging and scaling steps. b) $2F_{obs} - F_{calc}$ electron density map along the retinal chromophore and Lys205 using Careless [79]. c)$2F_{obs} - F_{calc}$ electron density map of TM2 of the transducer (Residues $54 - 82$) using raditional merging and scaling steps. d)$2F_{obs} - F_{calc}$ electron density map of TM2 of the transducer using careless. These maps are contoured at 1.6σ and generated using Pymol.

This machine learning processing improved the resolution from 3.4 Å to 2.85 Å (Fig.4.1). Phenix [99] has been used for the molecular replacement and the phases have been taken from PDB entry 1H2S [9]. For the structure refinement we used Phenix and Coot [100]. Comparing key regions from the structure scaled and merged with conventional methods (Fig.4.1a,c) to the one scaled and merged with Careless (Fig.4.1b,d), a more continuous electron density around the retinal as well as more defined electron density surrounding the transducer side chains, can be observed using the new method. Our results suggest Careless to be a good tool to improve the quality and resolution of low resolution serial synchrotron X-ray crystallography data.

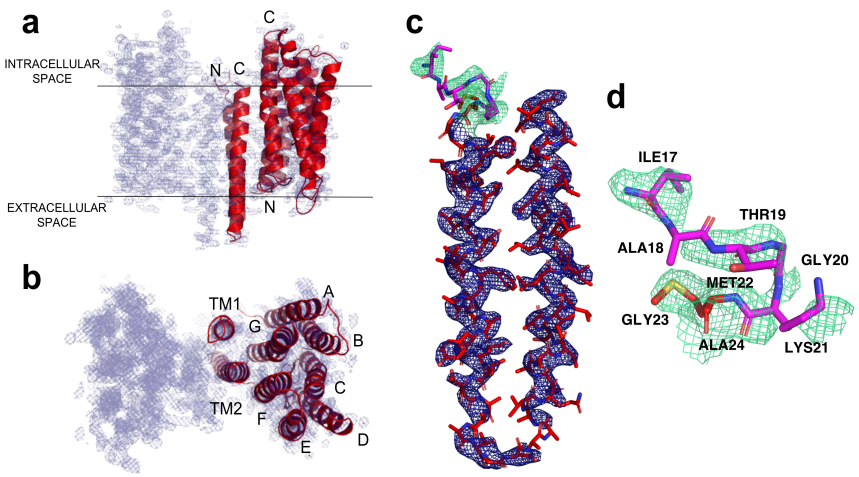

Figure 4.2: Sensory Rhodopsin II with its transducer HtrII. a) Front view of the complex where just the asymmetric unit is shown. b) Top view of the asymmetric unit with the helices from SRII (A-F) and HtrII (TM1 and TM2) are labelled. c) Side view of the transducer. $2F^{obs} - F^{calc}$ composite omit electron density map (blue contoured at 1.6 σ, green contoured at 0.7 σ. d) Close up view of the additional residues and the composite omit map.

4.1.3 Extended electron density for TM2 of HtrII

Previously deposited structures modelled residues from Met22 to Gly84 (Fig.4.4) [24], [29], [97], [101]. Our SSX data enabled us to model five more residues (Ile17, Ala18, Thr19, Gly20, Lys21) at the cytoplasmic end of TM1. Although the electron density in this region starts to be weaker from Gly23, the density is still well defined and continuous (Fig.4.2c,d). There is no electron density for residues from 1 to 21, and others have predicted that this region is disordered. Moreover, from residue 17 to 21 there is no clear α-helical secondary structure. We observe Met22 to form a H-bond with the backbone nitrogen of Val25. We can speculate that some water-mediated H-bonds may connect these residues to the SRII charged residues where also Asp214 is present, but our 2.85 Å does not allow us to observe putative water molecules.

4.1.4 Complex structure

The protein complex is a dimer with a two-fold symmetry axis between the transducers (Fig.4.2a,b). Our SSX data confirm the previously observed hydrogen bond network and the electrostatic interactions connecting SRII to its transducer [27]. In particular, we could observe hydrogen bond networks between helix F and helix G of SRII with the TM helices of the transducer, both in the intracellular side (Arg162 with Ala80 and Leu82), in the transmembrane region (Tyr199 with Asn74), and in the extracellular side (Thr189 with Ser62 and Glu43) (Fig.4.3a,b,c). Flash photolysis data have shown the importance of Tyr199 [26], [102], [103] as a key residue involved in the binding between SRII and its transducer [102]. Previous SRII data at cryogenic temperature have revealed a charged surface on the cytoplasmic side of helices F (Lys157, Ser158, Arg162, Arg164, and Asn165) and G (Asp214) on SRII, that is believed to interact electrostatically with the negatively charged cytoplasmic domain Gly101-Asp102-Gly103-Asp104-Leu105-Asp106 (not shown) of HtrII TM2 [27], [102]. Our SSX data further confirmed the electrostatic surface on SRII (Fig.4.3d).

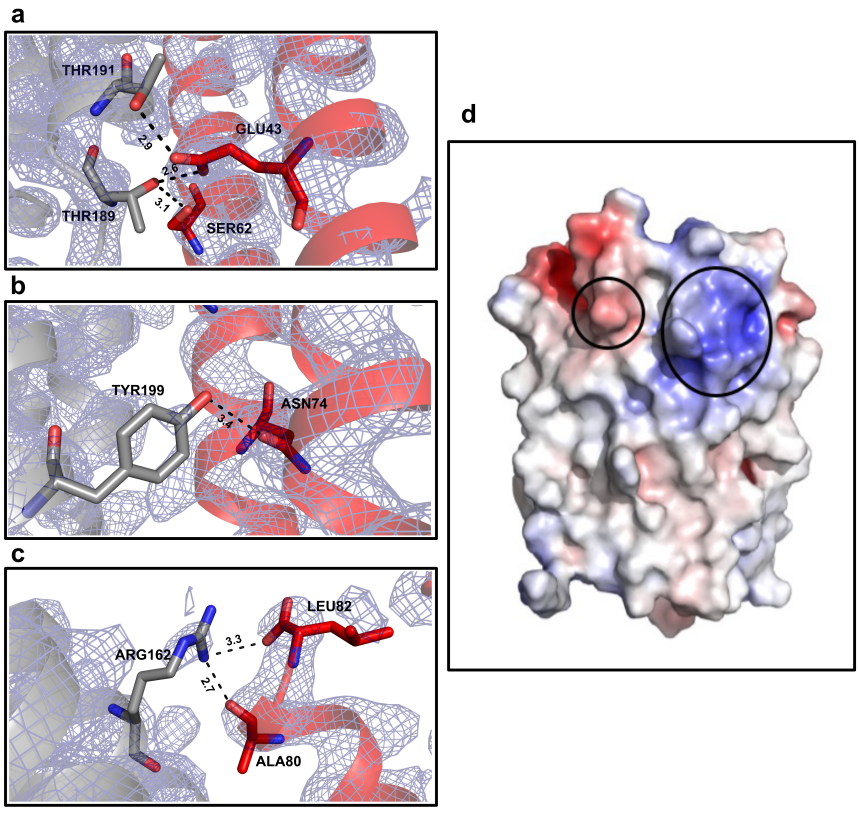

Figure 4.3: Hydrogen bonds interactions between helix F and G of SRII and TM1 and TM2 of HtrII. a) Extracellular side of the complex. b) Transmembrane domain. c) Intracellular side of the complex. All the residues and the bond lengths are labelled accordingly. d)Electrostatic surface potential on SRII, helices F and G. The residues in the large oval are Lys157, Ser158, Arg162, Arg164, Asn165 on helix F, and in the small oval Asp214 on helix G.

4.1.5 U/V shaped quaternary structures

Previous deposited structures suggest a "U" and "V" quaternary conformation of the complex based upon the angle and the position of the protomers [24], [29], [101]. The "U" conformation is observed in SRII:HtrII structures in their ground state and is characterised by a tighter contact

between SRII and its transducer impeding the movement of TM2 [25], [103]. This conformation is suggested to make it impossible to transmit the signal [24] to the AS1 helix of the HAMP domain which protrudes perpendicular to TM2 of the Sensory Rhodopsin transducer [104], [105]. Published photoactivated structures (PDB 5JJN [24], 2F95, 2F93 [29], 1H2S [9]) instead, show the protein complex into a "V" shape. The "V" shape is described by the symmetric monomers distancing each other on the cytoplasmic side while staying close on the extracellular side. The switch between the two conformations is hypothesized to be associated to the signal transmission from SRII to HtrII [24], and consequently to the HAMP domain, but the mechanism is still to be clarified. We superimposed our complex structure with PDB entry 5JJE (in "U" conformation) and PDB entry 1H2S (in "V" conformation) and confirmed the inactive state of our protein complex (Figure not shown).

4.1.6 Hierarchical clustering analysis of structures of the SRII:HtrII complex

Internal distance matrices have been calculated to correlate our SRII:HtrII complex structure with the others previously deposited. The internal distance matrix is not affected by the distribution of the atoms in space and no alignment is needed [106]. We analysed the data from peviously published structures using their deposited PDB files. We then calculated the distance between $C\alpha$ atoms between pairs of PDBs and calculated the scoring function (S_{ij}) to assess the absolute values of all elements within the difference internal distance matrix. We clustered the resulting values corresponding to each PDB in a dendrogram. The structures are ordered based on the (S_{ij}), where the lower the value the shorter the distance, and sorted the structures based on their similarity [107]. In Figure 4.4a we focused on the whole complex, while in figure 4.4b we targeted the transducer alone. When the whole complex is considered, our structure is clustered separately from the other structures. We can speculate that it can be due to our structure being the only one collected at room temperature or to a different space group. When the transducer is considered alone, it will cluster with the others based on space group similarities attesting to the importance of the crystal packing in the clustering.

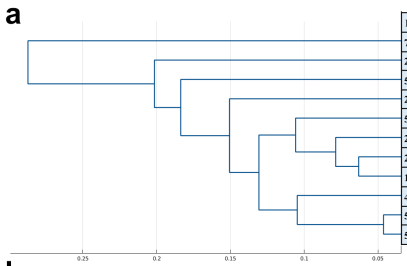

PDB code	Author	Space Group	Conformation	Resolution Å	HtrII Start-end
7ZCM	Ortolani	P 2_1 2 2	U	2.85	Ile17 - Leu82
2F93 - K	Moukhametzianov	$P2_12_12$	K	2	Val29 - Ala79
5JJJ	Ishchenko	$P6_4$	U	2.5	Gly23 - Leu82
2F95 - M	Moukhametzianov	$P2_12_12$	M	2.2	Ile27 - Ala79
5JJN	Ishchenko	$P2_12_12_1$	V	2.25	Gly23 - Phe83
2F93 - U	Moukhametzianov	$P2_12_12$	U	2	Val29 - Ala79
2F95 - U	Moukhametzianov	$P2_12_12$	U	2.2	Ile27 - Ala79
1H2S	Gordeliy	P21212	V	1.93	Gly23 - Leu82
4GYC	Ishchenko	$I2_12_12_1$	U	2.05	Gly23 - Phe83
5JJF	Ishchenko	$I2_12_12_1$	M	1.9	Met22 - Gly84
5JJE	Ishchenko	$I2_12_12_1$	U	1.9	Met22 - Gly84

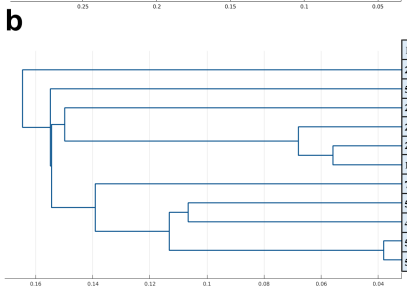

PDB code	Author	Space Group	Conformation	Resolution Å	HtrII Start-end
2F93 - K	Moukhametzianov	$P2_12_12$	K	2	Val29 - Ala79
5JJJ	Ishchenko	$P6_4$	U	2.5	Gly23 - Leu82
2F95 - M	Moukhametzianov	$P2_12_12$	M	2.2	Ile27 - Ala79
2F93 - U	Moukhametzianov	$P2_12_12$	U	2	Val29 - Ala79
2F95 - U	Moukhametzianov	$P2_12_12$	U	2.2	Ile27 - Ala79
1H2S	Gordeliy	P21212	V	1.93	Gly23 - Leu82
7ZCM	Ortolani	P 2_1 2 2	U	2.85	Ile17 - Leu82
5JJN	Ishchenko	$P2_12_12_1$	V	2.25	Gly23 - Phe83
4GYC	Ishchenko	$I2_12_12_1$	U	2.05	Gly23 - Phe83
5JJF	Ishchenko	$I2_12_12_1$	M	1.9	Met22 - Gly84
5JJE	Ishchenko	$I2_12_12_1$	U	1.9	Met22 - Gly84

Figure 4.4: Hierarchical clustering of SRII:HtrII complex. a) Dendrogram where the whole complex has been analysed. b) Dendrogram where just the transducer HtrII has been analysed.

4.1.7 Discussion

Recent advances with the performance of Synchrotrons and X-FELs opened new opportunities for structural biology. New opportunities are also given due to the possibility to observe conformational changes over time at room temperature.

Here we reported the SSX data collected at room temperature of the SRII:HtrII complex in its ground state. We have been able to confirm the structural features observed at cryogenic temperatures, and we have been able to model five additional residues on TM1. We aim in the future to optimise the crystallisation conditions of the SRII:HtrII and to collect data to an X-FEL to get a better resolution.

Chapter 5

Paper III

5.1 Serial crystallography structure of the light-activated Sensory Rhodopsin II:transducer complex.

When light is perceived by SRII, the signal is transmitted by a tight interaction to its transducer HtrII. This triggers the start of the TCS signalling cascade (Fig.1.4) that controls a photophobic reaction of *N.pharaonis* to blue light [108]. The photocycle in SRII is characterised by multiple helical displacements, but the most important for the signal transmission is the outward movement of helix F in SRII [9], [103]. Thaw/freeze-trapping studies suggested that the transducer senses the helix F displacement and moves its TM2 upwards in a piston-like movement transmitting the signal into the HAMP domain [24], [29], [109]. This in turn phosphorylates CheA and CheW which phosphorylate CheY, causing either the activation of the flagellar motor or the feedback response [110]. High-resolution structures of SRII alone and in complex with HtrII have given insights into their molecular structure. Thaw/freeze-trapping and TR-SSX studies have been conducted on SRII alone, while EPR, FTIR and Thaw/freeze-trapping studies have been conducted on SRII in a complex [24], [29], [35], [91]. The measured $C\alpha$ displacements from Pro144 to Pro175 of helix E and F are 0.34 Å in PDB entry 2F95, 0.47 Å in PDB entry 5JJF, and 0.78 Å in PDB entry 3QDC, suggest that the full extent of protein motions are not always captured in the thaw/freeze-trapping method. The same investigations have been conducted also in bR [31], [77], [81], [107], [111]–[113]. Here we present a room temperature SSX structure of the

photostationary state from continuously illuminated SRII:HtrII microcrystals. We show stacked positive and negative difference Fourier electron density peaks extending from the retinal to the SRII:HtrII interface. Our aim is to clarify how the signal propagates from SRII to HtrII. We show the displacement of Trp171 of helix F of SRII upon retinal isomerisation and how this may be sensed by the transducer. As with the low-temperature thaw/freeze-trapping studies, we also observe small $C\alpha$ displacements.

5.1.1 X-ray diffraction data collection and spectroscopic analysis

Microcrystals were transported to the Swiss Light Source and data were collected at room temperature. The sample viscosity was optimised by adding 20-25% of monoolein to the crystals in LCP. The sample was extruded from the high viscosity injector designed by Arizona State University [75] having a $75\mu m$ nozzle diameter with a sample flow rate of 40 nl/min. A continuous laser was used to illuminate the sample as it passed through the X-ray beam, using the same experimental geometry as described in **Paper I**. The laser was focused onto the sample with a focal spot 75 m $\times$ 75 m. The measured laser power on the sample was 2.6 mW at 488 nm in wavelength. The X-ray and laser beam were aligned to overlap. We estimate that the transit time of the sample through the laser was such that, on average, each crystal was illuminated the order of 240 ms. X-ray diffraction data were collected at 50 Hz on a 16 M hybrid pixel detector. The X-ray energy was 12.4 keV focused to a spot size 20 m horizontal and 5 m vertical.

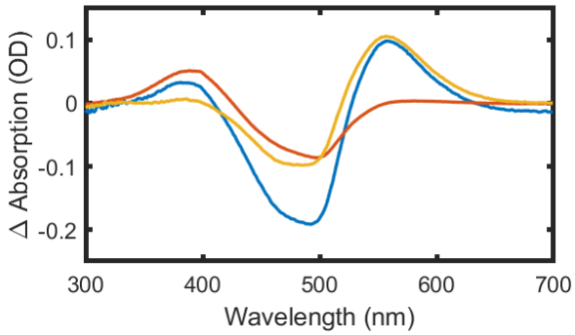

Figure 5.1: UV-Vis analysis of SRII in LCP. Spectrum measured for 240 ms at 478nm (blue line). 37% of the photoactive SRII is in M-state (red) and 63% in O-state (mustard). The capillary size is 0.35 mm.

Because of the kinetics associated with the later intermediates, we expect to see structures in M and O conformations to coexist in the same time. This is confirmed by UV-Vis spectroscopy on SRII, where solubilized protein in the crystallization conditions have shown 50% of photoactivation (while TR-SSX tends to have a lower percentage of photoactivation) of which the 37% was in the M-state and the 63% was in the O-state (Fig.5.1).

5.1.2 Overview of protein conformational changes

In our calculated difference Fourier electron density map we can observe stacked difference electron density peaks with paired positive and negative density expand from the retinal to helix E and F. On figure 5.2A the difference electron density features are more intense around the retinal and become weaker and more noisy as the distance from the retinal increases [31], [93], [107], [112], [114]. This is due to a steric clash between the C20 methlyl group of 13-*cis* retinal and Trp171 in SRII that causes an outward movement of helix F. Other positive and negative density arise from Trp73 on the extracellular side of retinal towards the extracellular interface between helices F and G of SRII and both TM1 and TM2 of HtrII. Difference electron density features are still very clear on the cytoplasmic

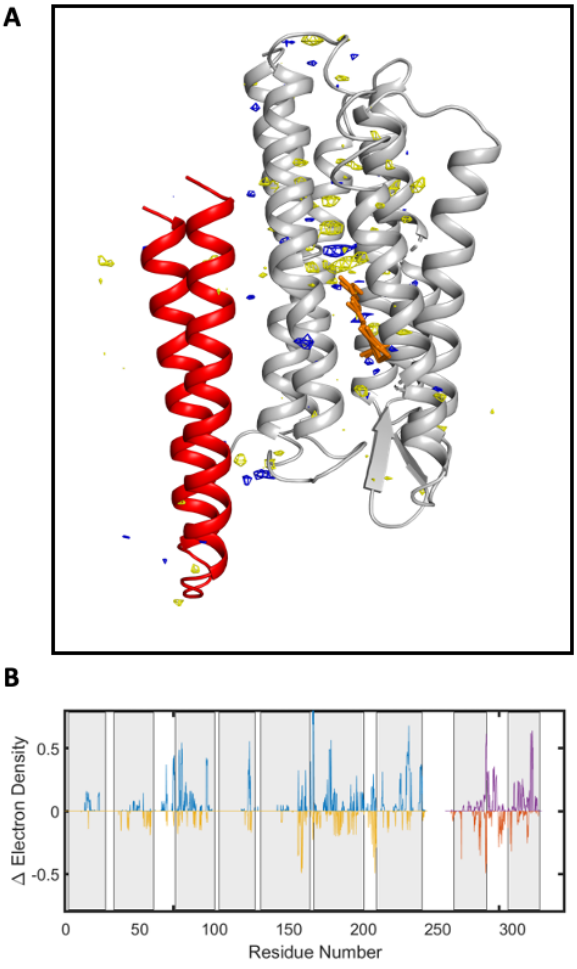

Figure 5.2: A) Light-induced changes in electron density. In blue positive difference electron density and yellow mesh indicating negative difference electron density. This figure is contoured at $\pm$ 4.0 σ, where σ is the root mean square electron density of the unit cell. B) Difference Fourier electron density map whereby changes in electron density are quantified atom-by-atom and then plotted versus the atom-number in the pdb file. Data from SRII are calculated using a sphere of integration with radius 3.0 Å and a pedestal floor of 3.6 σ, whereas that for HtrII are calculated using a sphere of integration with radius 3.0 Å and a pedestal floor of 3.2 σ.

portion of helix E, on helix F, on the extracellular loop of TM2 and partially on the cytoplasmic side of TM1(Fig.5.2B) [90].

5.1.3 Conformational changes propagate from isomerised retinal towards both sides of SRII

Our difference Fourier electron density map shows helical displacements on both the cytoplasmic and the extracellular side of helix F. The retinal isomerisation causes a steric clash between its C20 and Trp171 with the latter moving towards the cytoplasm. This movement creates a clash with Thr167 that gets displaced and in turn clashes with Leu163 (Fig.5.3A). These stacked electron density differences reveal the cascade of events that reflect the helix F movement. On the extracellular side of the retinal, Trp76 (helix C) moves towards the cytoplasm upon retinal isomerisation. This creates a structural perturbation that affects Tyr73 which influences the conformation of Trp178 (Helix F) to which it forms a H-bond.

5.1.4 Conformational changes on the extracellular side of the SRII:HtrII complex

Trp178 on helix F has stacked paired positive and negative features that continue down to Leu187 and Thr189 on the extracellular side of helix G (5.3B). Thr189 forms a H-bond with Glu43 (TM1) and Ser62 (TM2). Glu43 together with Phe36, has paired positive and negative difference electron density features that extend from Leu187 through Pro190 and to Ala195 suggesting a coordinated outward movement of the SRII F-G loop which conveys a signal to TM1. This electron density is also very clear in figure 5.2A and has not been described in earlier freeze-trapping experiments [24], [29], [35].

5.1.5 Conformational changes on the cytoplasmic side of the SRII:HtrII complex

On the cytoplasmic side of the complex, difference electron density expands from helix F to the transducer (Fig5.3C). Strong difference electron density is observed for Trp171 and Thr167 and weak difference electron

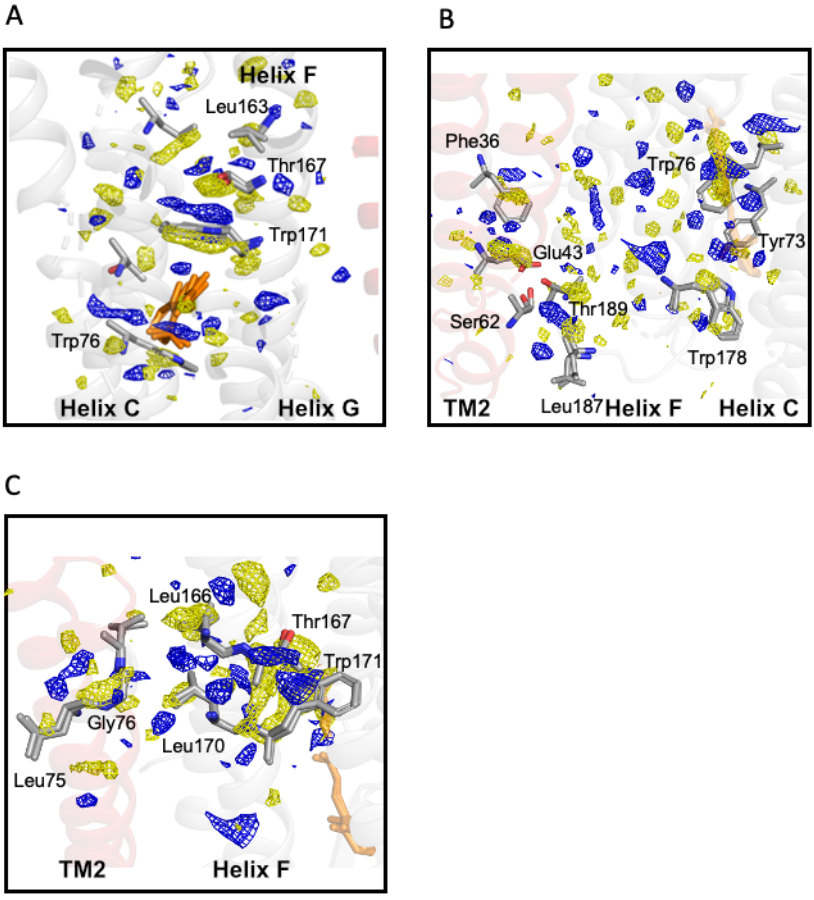

Figure 5.3: Propagation of difference electron density features away from the retinal and towards HtrII. A) Difference density changes stacking both on the extracellular side of retinal (Trp76) and on the cytoplasmic side of the retinal (Trp171, Thr167 and Leu163). B) Difference electron density features on the extracellular portions of helix F (Trp178) and onto TM2 of HtrII (Glu43). C) Difference electron density features on the cytoplasmic portions of helix F (Leu166 and Leu170) and into TM2 of HtrII (Leu75 and Gly76). Blue mesh indicates positive difference electron density and yellow mesh indicates negative difference electron density.

density is present on Leu170 and Leu166. More difference electron density is shown on Leu75 and Gly76 (TM2) which appears to indicate a movement of TM2 away from SRII. In the dark state, Tyr199 (helix G) forms a H-bond with Asn74, and this H-bond remains in the photoilluminated state. Also, on the cytoplasmic side of helix F, there are the charged residues Arg162, Arg164 and Asp165 having difference electron density peaks suggesting movements. To conclude, the interaction between Arg162, Ala80 and Thr81 gives a weak density on TM2, but more analysis is needed to extract a convincing movement.

5.1.6 Structural refinement of changes in helix F of SRII and TM2 of HtrII

To analyse how the signal is transmitted from SRII to HtrII, we performed a preliminary analysis on the region that includes helices E and F, and the extracellular side of helix G (including Lys205)) of SRII by selecting the residues from Gly120 (D-E loop on extracellular side) to Gly 207 (helix G). We did the same with HtrII, selecting residues from Gly42 in the extracellular loop up to Leu82 (Fig.5.4B). These regions were assigned with a 30% occupancy in their photoactive conformation and were free to rearrange during the refinement process, while the complementary conformation, corresponding to the dark structure, was assigned with a 70% occupancy and was held fixed. The other SRII:HtrII residues not mentioned, were given a 100% occupancy and were held fixed. A preliminary analysis of the $C\alpha$-atoms displacements shows a displacement of 0.31 Å for the above mentioned C-α atoms, both in SRII and HtrII (Fig.5.4A,B). On the region from Pro144 of helix E to Pro175 of helix F which includes Trp172, the residues are displaced upon retinal isomerisation with a rmsd is 0.38 Å (Fig.5.4B). On the cytoplasmic side of helices E and F there is the biggest $C\alpha$-atoms displacement, and its extension is comparable to freeze-trapped deposited structures, some of which have an even more extended movement. A net displacement of 0.12 Å is observed towards the cytoplasm of TM2 and is consistent with the piston-like movement previously suggested [24], [29], [108]. In contrast, the 15° rotation of TM2

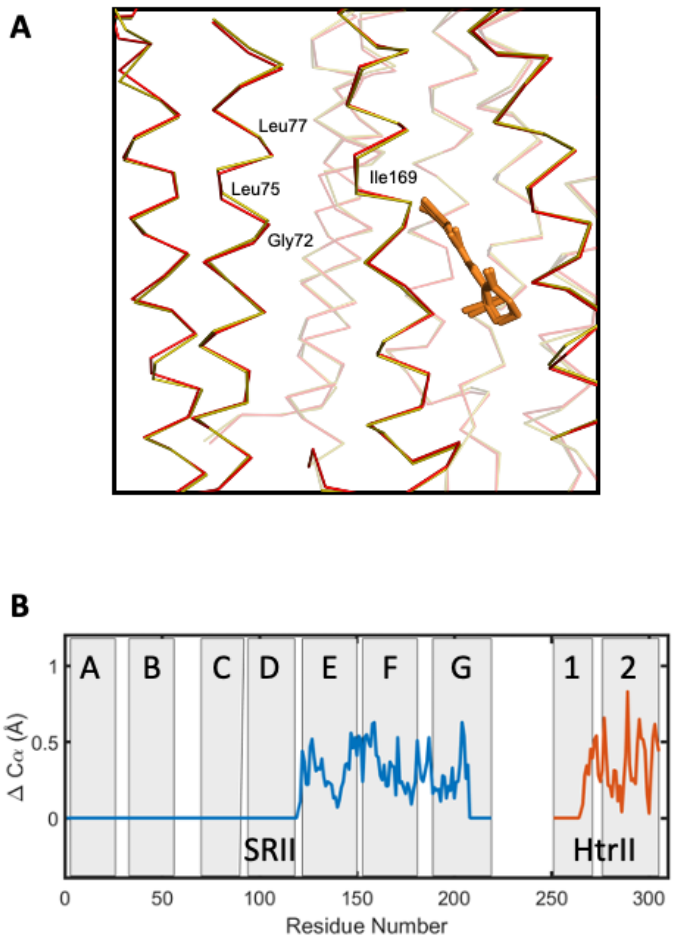

Figure 5.4: A) Preliminary conformational changes on helices E and F of SRII and TM2 of HtrII. In red the resting conformation and in mustard the light-activated. B)Root mean square displacements of Cα atoms. From Gly120 of loop D-E on the extracellular side to Gly207 of helix G were assigned an occupancy of 30% in the light-activated structure while the complementary residues have an occupancy of 70%. The same on TM2 from Gly42 to Leu82.

[29], seems more reduced in our TR-SSX data and appears to rotate towards the opposite direction. Further analysis needs to be done to assess

the details of this rotation.

5.1.7 Conclusions

TR-SSX is a new method in structural biology to observe time-resolved conformational changes within proteins. Previous studies on bR have shown high levels of consistency between cryo-crystallography and TR-SSX, although in one study a more extensive helical displacement was observed when using TR-SSX [93], [107], [113].

Our SRII:HtrII data are consistent to the thaw/freeze trapping, but we do not observe a larger helical displacement when using TR-SSX. We can speculate that the reason for this to may be due either to a smaller helical displacement required by the HAMP domain to sense the signal, or to the crystal constraints that may limit the extent of the movement. The difference Fourier electron density maps showed how the signal propagation happens on both the intracellular and the extracellular sides of the complex, with a difference electron density on the F-G extracellular loop and connected movements of TM1 and TM2. A preliminary helical displacement analysis shows a very subtle movement of TM2.

Chapter 6

Paper IV

6.1 Time-resolved X-ray solution scattering observations of light induced structural changes in Sensory Rhodopsin II

Time-resolved X-ray solution scattering (TR-XSS) is an experimental approach to study conformational changes of proteins in solution. TR-XSS does not give direct information on the structure at atomic resolution as crystallography does, but it is a complementary method, which can help us make the structural observations from proteins, especially when combined with molecular dynamics simulations [115]–[121] and cryo-crystallography [13], [94], [115]. In this paper we investigate how light triggers conformational changes in *N.pharaonis* SRII, elucidating similarities and differences with bR, and we analyse the differences when SRII is alone or bound to its transducer. In our TR-SSX data (**Paper I**) and SSX data (**Paper III**) we could observe an outward movement of helices E and F, as well as bigger displacements with helices C, D and E in their extracellular regions. As previously discussed in this thesis, the extent of the movements when the transducer is present is reduced in helices E and F (**Paper III**). The goal of this study is to elucidate the extent of the helical displacements in SRII in isolation and when the transducer is bound to SRII using TR-XSS.

6.1.1 Time-resolved X-ray scattering difference data

Data have been collected at the beamline ID09B of the European Synchrotron Radiation Facility (ESRF). Sample was illuminated at $\lambda = 450nm$

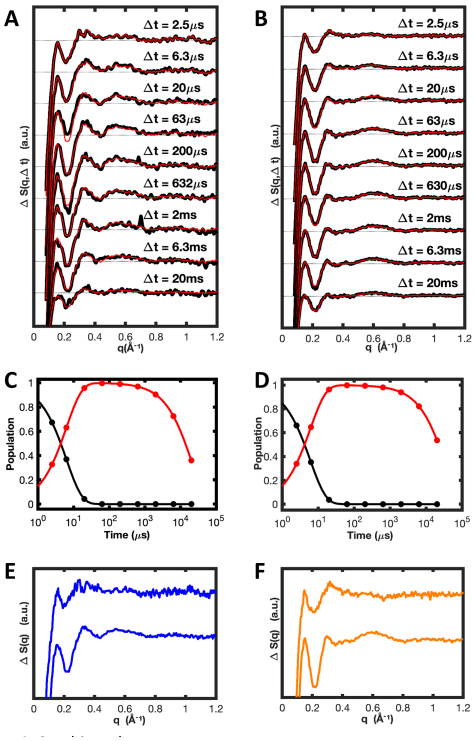

Figure 6.1: Experimental difference X-ray scattering curves recorded from photoactivated SRII and SRII:HtrII. A) Time-dependent changes in X-ray scattering associated with SRII in isolation. B) Time-dependent changes in X-ray scattering associated with the SRII:HtrII complex. The black line represents experimental data and the red line the reconstructed data from the basis spectra (panels E and F) recovered by linear decomposition. C) Population of the two components extracted by linear decomposition of the SRII TR-XSS data that were used to generate the basis spectrum in panel E, and the reconstructed data (red lines) in panel A. D) Population of the two components extracted by linear decomposition of the SRII:HtrII TR-XSS data that were used to generate the basis spectrum in panel F, and the reconstructed data (red lines) in panel B. E) Basis spectra showing the early component (top, State 1, $SRII_{S1}$) and later component (bottom, State 2, $SRII_{S2}$) extracted by linear decomposition of the SRII TR-XSS data. F) Basis spectra showing the early component (top, State 1, $SRII : HtrII_{S1}$) and later component (bottom, State 2, $SRII : HtrII_{S2}$) extracted by linear decomposition of the SRII:HtrII TR-XSS data.

(pump) and the exposure (probe) was $2\mu s$ for the time delays $\Delta t \leq 6.3\mu s$ and $20\mu s$ for time delays with $\Delta t \geq 20\mu s$, where Δt represents the time of arrival of the X-ray pulse-train following photo-excitation. Time-delays collected are at $\Delta t = 2.5\mu s, 6.3\mu s, 20\mu s, 63\mu s, 200\mu s,\ 630\mu s, 2ms, 6.3ms,$ and $20ms$, and a control at $-30\mu s$. The difference X-ray scattering curves are shown in Figure 6.1A for SRII and Figure 6.1B for SRII:HtrII [94].

6.1.2 Linear decomposition of the difference X-ray scattering data

Linear decomposition has been executed on the data. Both SRII and SRII:HtrII data have been divided in two populations of 2 components called State 1 and State 2 (Fig.6.1C,D). This procedure assumes a exponential rise and decay for all intermediates [94]. The population in State 1 (in black) starts with a population of 1 and decays exponentially with a time-constant $\tau 1$ while the population 2 (in red) increases with a time-constant $\tau 1$ and decays with a time constant $\tau 2$. Their basis spectra are represented in figure 6.1E and F, respectively for SRII and for SRII:HtrII. The basis spectra shown are very similar for State 1 in both cases, revealing that independently of the presence of the transducer, the early conformational changes are identical within the noise of these data. Also, the decay time-constant represents the time necessary to clear the illuminated sample from the X-rays. In this case the time-differences for $\tau 2$ are due to different experimental geometries and flow-rates used in the two experiments. A comparison has been made with bR data, where the spectrum has been divided in 3 components both from TR-XSS and TR-SFX [94]. It suggests that the same structural change happens in bR with a time-constant of $20\mu s$ as well as in for both SRII alone and in complex. Since structural changes happen at approximately the same timing as the SB deprotonation, in their respective photocycles, this may be the cause-effect reaction between the SB deprotonation and the conformational changes [93], [122].

6.1.3 Structural modelling of X-ray scattering changes

A comparison of the X-ray scattering curves between State 2 of SRII and bR have shown identical curves for later q, demonstrating similar conformational changes in both the proteins. In shorter q, the difference may due to the micelle packing, or different pH or different concentration of counter ions. We modeled conformational changes observed on the scattering of $SRII_{S2}$, $SRII : HtrII_{S1}$ and $SRII : HtrII_{S2}$ with Gromacs [123] and then we got theoretical difference scattering curves with Crysol [124]. In SRII we focused on the same helical regions of C (Phe69 to Leu82), D, E (Val107 to Phe127) and F observed in TR-SSX studies of SRII (**Paper I**). We scaled the movements and gave energy constraints for the molecular dynamics and the scattering has been predicted for the protein alone, the micelle alone, and the protein plus detergent micelle. The micelle structural fluctuation and the influence of the solvent was taken into account.

The mean displacements of $C\alpha$ atoms calculated for $SRII_{S2}$, $SRII : HtrII_{S1}$ and $SRII : HtrII_{S2}$ from molecular dynamics for Pro144 to Pro175 are comparable with the X-ray structure of SRII refined from TR-SSX data captured 30 ms after photoactivation while from Phe69 to Leu82 and the extracellular portions of helices D and E from Val107 to Phe127 are smaller (Fig.6.2E).

To conclude, the fitting of the TR-XSS data recovered from SRII in isolation and in complex with its transducer protein reveal an outwards movement of the cytoplasmic portions of helices E and F, reduced when SRII is bound to its transducer, smaller than what observed for bR but larger than using serial crystallography (Fig.6.2). These data are also consistent with the displacement of the extracellular regions of helices C, D and E, but lower than recovered in the TR-SSX structure.

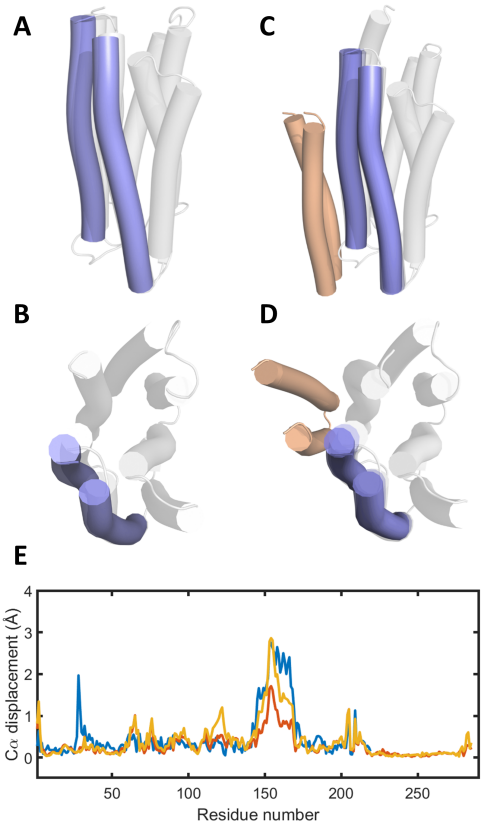

Figure 6.2: Schematic overview of light-induced structural changes in SRII in isolation and the SRII:HtrII complex. A) Superposition of the SRII resting model (gray) and the results from fitting $SRII_{S2}$, when viewed from the plane of the membrane. B) Same as A, top view. C) Superposition of the SRII resting model (gray) and the results from fitting $SRII : HtrII_{S2}$, when viewed from the plane of the membrane. D) Same as C, but top view. E) Root mean square displacements of $C - \alpha$ atoms resulting from sampling those molecular dynamics conformations which best fit the difference X-ray scattering data. Blue: the mean displacements of $C - \alpha$-atoms when fitting SRIIS2. Red: the mean displacements of $C - \alpha$-atoms when fitting SRII:HtrIIS1. Mustard: the mean displacements of $C - \alpha$-atoms when fitting SRII:HtrIIS2. In this plot SRII is from residue 1 to 219, whereas HtrII is from residue 220 to 285.

6.1.4 Conclusions

Light has a critical role for the survival in many organisms. When the light-signal is absorbed by the retinal, the signal is amplified and propagates along the protein initiating a photocycle. We collected TR-XSS data to better understand the mechanisms of signal propagation in both SRII alone and in a complex. We observed that in both SRII and SRII:HtrII the basis spectra are indistinguishable within noise but they diverge at later times. Structural modelling against these data show a 30% larger extent in the movement of helices E and F when SRII is not bound to its transducer.This has been confirmed by EPR experiments both in bR and in SRII [96], [125]. This may explain the interruption of the proton movements when HtrII is present. In general, SRII alone has more extended movements than when bound with HtrII. Also, as also happened with bR, the extent of $C\alpha$ displacements in solution recovered by structural fitting is larger than in TR-XSS.

Chapter 7

Conclusions and future perspectives

The outcome of these experiments will lead to the submission of the manuscripts included in this thesis.

On Paper I we focused on the two microbial rhodopsins Sensory Rhodopsin II and Bacteriorhodopsin. Despite structural similarities, their photocycle differs in time-duration. We compared time-resolved serial synchrotron X-ray crystallography (TR-SSX) datasets of both proteins and analysed the structural features, helical movements and water displacements. Our data explained the connection between the different photocycle duration and their function, respectively a phototactic sensor and proton pump. Very recently SRII TR-XSS data have been collected at the Swiss Light Source. A preliminary analysis shows a higher resolution data of the crystals and improved time-resolution. This may allow us to have shorter time-points and to better characterise the evolution of the photocycle with this method. In Paper II we introduced a new strategy to observe Sensory Rhodopsin II with its transducer HtrII, complementing the cryo-crystallography with a room temperature serial synchrotron X-ray crystallography (SSX) approach. We have been able to apply a new scaling and merging method which improved the resolution of our serial crystallography structure. Our data confirmed the same structural features previously published using cryo-crystallography, but allowed five additional residues to be built on the cytoplasmic side of the TM1 of the transducer. Further improvements of the crystallisation conditions may lead to a better resolution of the complex. In paper III, TR-XSS data on

the photoactive state of the complex have been collected at the Swiss light Source. A preliminary analysis of the light-activated complex structure gave us interesting insights on the signal transmission and the extent of the movements. Further refinement is required to improve the quality of the structure and draw stronger conclusions. In paper IV we collected TR-SSX data from both SRII and the complex and together with Gromacs simulations, we observed a more extended helical movement than in TR-XSS or in cryo-trapping studies.

Better diffracting microcrystals of the SRII:HtrII complex may yield a better resolution structure and more insights about serial crystallography water displacements when SRII is bound to its transducer. A time-resolved data collection from the complex may better explain the time-resolution and extentof the helical displacements. Furthermore, the whole length transducer has never been crystallised. Future attempts to crystallize protein produced using a more extended construct may lead to a better understand on the helical movements of the transducer. Also, due to the difficulty to crystallise the full-length transducer and to crystallise the SRII:HtrII complex together with the HAMP domain, more attempts using solution scattering or cryo electron microscopy may prove a better strategy to elucidate how the signal transmission to the HAMP domain is performed.

Bibliography

[1] A. Breda, N. F. Valadares, O. N. d. Souza, and R. C. Garratt, "Protein Structure, Modelling and Applications," Sep. 2007. [Online]. Available: https://www.ncbi.nlm.nih.gov/books/NBK6824/.

[2] A. Pandey, K. Shin, R. E. Patterson, X. Q. Liu, and J. K. Rainey, *Current strategies for protein production and purification enabling membrane protein structural biology1*, 2016. DOI: 10.1139/bcb-2015-0143. [Online]. Available: https://pubmed.ncbi.nlm.nih.gov/27010607/.

[3] R. Reis and I. Moraes, "Structural biology and structure-function relationships of membrane proteins," *Biochemical Society transactions*, vol. 47, no. 1, pp. 47–61, 2019, ISSN: 1470-8752. DOI: 10.1042/BST20180269. [Online]. Available: https://pubmed.ncbi.nlm.nih.gov/30559269/.

[4] A. V. Guzzo, "The influence of amino-acid sequence on protein structure," *Biophysical journal*, vol. 5, no. 6, pp. 809–822, 1965, ISSN: 0006-3495. DOI: 10.1016/S0006-3495(65)86753-4. [Online]. Available: https://pubmed.ncbi.nlm.nih.gov/5884309/.

[5] L. E. Hedin, K. Illergård, and A. Elofsson, "An introduction to membrane proteins," *Journal of Proteome Research*, vol. 10, no. 8, pp. 3324–3331, Aug. 2011, ISSN: 15353893. DOI: 10.1021/pr200145a. [Online]. Available: https://pubs.acs.org/sharingguidelines.

[6] S. J. Singer and G. L. Nicolson, "The fluid mosaic model of the structure of cell membranes," *Science*, vol. 175, no. 4023, pp. 720–731, Feb. 1972, ISSN: 00368075. DOI: 10.1126/science.175.4023.720. [Online]. Available: http://science.sciencemag.org/.

[7] H. Watson, "Biological membranes," *Essays in Biochemistry*, vol. 59, p. 43, Nov. 2015. DOI: 10.1042/BSE0590043. [Online]. Available: /pmc/articles/PMC4626904//pmc/articles/PMC4626904/?report=abstracthttps://www.ncbi.nlm.nih.gov/pmc/articles/PMC4626904/.

[8] G. M. Cooper, "Cell Membranes," 2000.

[9] V. I. Gordeliy, J. Labahn, R. Moukhametzianov, R. Efremov, J. Granzin, R. Schlesinger, G. Büldt, T. Savopol, A. J. Scheidig, J. P. Klare, and M. Engelhard, "Molecular basis of transmembrane signalling by sensory rhodopsin II-transducer complex.," *Nature*, vol. 419, no. 6906, pp. 484–7, Oct. 2002, ISSN: 0028-0836. DOI: 10.1038/nature01109. [Online]. Available: http://www.nature.com/articles/nature01109http://www.ncbi.nlm.nih.gov/pubmed/12368857.

[10] H. Lodish, A. Berk, S. L. Zipursky, P. Matsudaira, D. Baltimore, and J. Darnell, "Membrane Proteins," 2000. [Online]. Available: https://www.ncbi.nlm.nih.gov/books/NBK21570/.

[11] W. Cho and R. V. Stahelin, *Membrane-protein interactions in cell signaling and membrane trafficking*, May 2005. DOI: 10.1146/annurev.biophys.33.110502.133337. [Online]. Available: www.annualreviews.org.

[12] Y. Kang, O. Kuybeda, P. W. de Waal, S. Mukherjee, N. Van Eps, P. Dutka, X. E. Zhou, A. Bartesaghi, S. Erramilli, T. Morizumi, X. Gu, Y. Yin, P. Liu, Y. Jiang, X. Meng, G. Zhao, K. Melcher, O. P. Ernst, A. A. Kossiakoff, S. Subramaniam, and H. E. Xu, "Cryo-EM structure of human rhodopsin bound to an inhibitory G protein," *Nature*, vol. 558, no. 7711, pp. 553–558, Jun. 2018, ISSN: 0028-0836. DOI: 10.1038/s41586-018-0215-y. [Online]. Available: http://www.nature.com/articles/s41586-018-0215-y.

[13] E. Malmerberg, P. H. Bovee-Geurts, G. Katona, X. Deupi, D. Arnlund, C. Wickstrand, L. C. Johansson, S. Westenhoff, E. Nazarenko, G. F. Schertler, A. Menzel, W. J. De Grip, and R. Neutze, "Conformational activation of visual rhodopsin in native disc membranes," *Science Signaling*, vol. 8, no. 367, Mar. 2015, ISSN: 19379145.

DOI: 10.1126/scisignal.2005646. [Online]. Available: www.SCIENCESIGNALING.org.

[14] O. P. Ernst, D. T. Lodowski, M. Elstner, P. Hegemann, L. S. Brown, and H. Kandori, "Microbial and Animal Rhodopsins: Structures, Functions, and Molecular Mechanisms," *Chemical Reviews*, vol. 114, no. 1, pp. 126–163, Jan. 2014, ISSN: 0009-2665. DOI: 10.1021/cr4003769. [Online]. Available: http://pubs.acs.org/doi/10.1021/cr4003769.

[15] H. E. Kato, F. Zhang, O. Yizhar, C. Ramakrishnan, T. Nishizawa, K. Hirata, J. Ito, Y. Aita, T. Tsukazaki, S. Hayashi, P. Hegemann, A. D. Maturana, R. Ishitani, K. Deisseroth, and O. Nureki, "Crystal structure of the channelrhodopsin light-gated cation channel," *Nature*, vol. 482, no. 7385, pp. 369–374, Feb. 2012, ISSN: 00280836. DOI: 10.1038/nature10870. [Online]. Available: https://www.nature.com/articles/nature10870.

[16] J.-M. Kim, P. J. Booth, S. J. Allen, and H. Khorana, "Structure and function in bacteriorhodopsin: the role of the interhelical loops in the folding and stability of bacteriorhodopsin," *Journal of Molecular Biology*, vol. 308, no. 2, pp. 409–422, Apr. 2001, ISSN: 0022-2836. DOI: 10.1006/JMBI.2001.4603. [Online]. Available: https://www.sciencedirect.com/science/article/pii/S0022283601946030?via%3Dihub.

[17] G. Nagel, T. Szellas, W. Huhn, S. Kateriya, N. Adeishvili, P. Berthold, D. Ollig, P. Hegemann, and E. Bamberg, "Channelrhodopsin-2, a directly light-gated cation-selective membrane channel.," *Proceedings of the National Academy of Sciences of the United States of America*, vol. 100, no. 24, pp. 13 940–5, Nov. 2003, ISSN: 0027-8424. DOI: 10.1073/pnas.1936192100. [Online]. Available: http://www.ncbi.nlm.nih.gov/pubmed/14615590http://www.pubmedcentral.nih.gov/articlerender.fcgi?artid=PMC283525.

[18] F. Zhang, J. Vierock, O. Yizhar, L. E. Fenno, S. Tsunoda, A. Kianianmomeni, M. Prigge, A. Berndt, J. Cushman, J. Polle, J. Magnuson, P. Hegemann, and K. Deisseroth, "The microbial opsin

family of optogenetic tools," *Cell*, vol. 147, no. 7, pp. 1446–1457, Dec. 2011, ISSN: 10974172. DOI: 10.1016/J.CELL.2011.12.004/ATTACHMENT/EE187084-4112-479C-B427-2AECC8CEE28A/MMC1.PDF. [Online]. Available: http://www.cell.com/article/S0092867411015029/fulltexthttp://www.cell.com/article/S0092867411015029/abstracthttps://www.cell.com/cell/abstract/S0092-8674(11)01502-9.

[19] J. Soppa, "Two hypotheses - one answer," *FEBS Letters*, vol. 342, no. 1, pp. 7–11, Mar. 1994, ISSN: 00145793. DOI: 10.1016/0014-5793(94)80573-3. [Online]. Available: http://doi.wiley.com/10.1016/0014-5793%2894%2980573-3.

[20] B. Yan, T. Takahashi, R. Johnson, F. Derguini, K. Nakanishi, and J. L. Spudich, "All-trans/13-cis isomerization of retinal is required for phototaxis signaling by sensory rhodopsins in Halobacterium halobium," *Biophysical Journal*, vol. 57, no. 4, pp. 807–814, 1990, ISSN: 00063495. DOI: 10.1016/S0006-3495(90)82600-X. [Online]. Available: /pmc/articles/PMC1280781/?report=abstracthttps://www.ncbi.nlm.nih.gov/pmc/articles/PMC1280781/.

[21] E. Pebay-Peyroula, A. Royant, E. M. Landau, and J. Navarro, "Structural basis for sensory rhodopsin function," *Biochimica et Biophysica Acta (BBA) - Biomembranes*, vol. 1565, no. 2, pp. 196–205, Oct. 2002, ISSN: 0005-2736. DOI: 10.1016/S0005-2736(02)00569-2.

[22] J. L. Spudich and H. Luecke, "Sensory rhodopsin II: functional insights from structure," *Current Opinion in Structural Biology*, vol. 12, no. 4, pp. 540–546, Aug. 2002, ISSN: 0959-440X. DOI: 10.1016/S0959-440X(02)00359-7. [Online]. Available: https://www.sciencedirect.com/science/article/pii/S0959440X02003597?via%3Dihub.

[23] C. P. Zschiedrich, V. Keidel, and H. Szurmant, "Molecular mechanisms of two-component signal transduction," *Journal of molecular biology*, vol. 428, no. 19, p. 3752, Sep. 2016. DOI: 10.1016/J.JMB.2016.08.003. [Online]. Available: /pmc/articles/

PMC5023499//pmc/articles/PMC5023499/?report=abstracthttps://www-ncbi-nlm-nih-gov.ezproxy.ub.gu.se/pmc/articles/PMC5023499/.

[24] A. Ishchenko, E. Round, V. Borshchevskiy, S. Grudinin, I. Gushchin, J. P. Klare, A. Remeeva, V. Polovinkin, P. Utrobin, T. Balandin, M. Engelhard, G. Büldt, and V. Gordeliy, "New Insights on Signal Propagation by Sensory Rhodopsin II/Transducer Complex," *Scientific Reports 2017 7:1*, vol. 7, no. 1, pp. 1–10, Feb. 2017, ISSN: 2045-2322. DOI: 10.1038/srep41811. [Online]. Available: https://www.nature.com/articles/srep41811.

[25] J. P. Klare, V. I. Gordeliy, J. Labahn, G. Büldt, H.-J. Steinhoff, and M. Engelhard, "The archaeal sensory rhodopsin II/transducer complex: a model for transmembrane signal transfer," *FEBS Letters*, vol. 564, no. 3, pp. 219–224, Apr. 2004, ISSN: 1873-3468. DOI: 10.1016/S0014-5793(04)00193-0. [Online]. Available: https://febs.onlinelibrary.wiley.com/doi/full/10.1016/S0014-5793%2804%2900193-0https://febs.onlinelibrary.wiley.com/doi/abs/10.1016/S0014-5793%2804%2900193-0https://febs.onlinelibrary.wiley.com/doi/10.1016/S0014-5793(04)00193-0.

[26] H. Luecke, B. Schobert, J. K. Lanyi, E. N. Spudich, and J. L. Spudich, "Crystal structure of sensory rhodopsin II at 2.4 angstroms: insights into color tuning and transducer interaction," *Science (New York, N.Y.)*, vol. 293, no. 5534, pp. 1499–1503, Aug. 2001, ISSN: 0036-8075. DOI: 10.1126/SCIENCE.1062977. [Online]. Available: https://pubmed.ncbi.nlm.nih.gov/11452084/.

[27] A. Royant, P. Nollert, K. Edman, R. Neutze, E. M. Landau, E. Pebay-Peyroula, and J. Navarro, "X-ray structure of sensory rhodopsin II at 2.1-A resolution," *Proceedings of the National Academy of Sciences of the United States of America*, vol. 98, no. 18, pp. 10 131–10 136, Aug. 2001, ISSN: 0027-8424. DOI: 10.1073/PNAS.181203898. [Online]. Available: https://pubmed.ncbi.nlm.nih.gov/11504917/.

[28] V. I. Gordeliy, J. Labahn, R. Moukhametzianov, R. Efremov, J. Granzin, R. Schlesinger, G. Büldt, T. Savopol, A. J. Scheidig, J. P. Klare, and M. Engelhard, "Molecular basis of transmembrane signalling by sensory rhodopsin II–transducer complex," *Nature 2002 419:6906*, vol. 419, no. 6906, pp. 484–487, Oct. 2002, ISSN: 1476-4687. DOI: 10.1038/NATURE01109. [Online]. Available: https://www-nature-com.ezproxy.ub.gu.se/articles/nature01109.

[29] R. Moukhametzianov, J. P. Klare, R. Efremov, C. Baeken, A. Göppner, J. Labahn, M. Engelhard, G. Büldt, and V. I. Gordeliy, "Development of the signal in sensory rhodopsin and its transfer to the cognate transducer," *Nature*, vol. 440, no. 7080, pp. 115–119, Mar. 2006, ISSN: 1476-4687. DOI: 10.1038/NATURE04520. [Online]. Available: https://pubmed.ncbi.nlm.nih.gov/16452929/.

[30] M. Engelhard and K. P. Hofmann, "Photoreceptors," in *Encyclopedic Reference of Genomics and Proteomics in Molecular Medicine*, Springer Berlin Heidelberg, Sep. 2006, pp. 1407–1413. DOI: 10.1007/3-540-29623-9{_}4410. [Online]. Available: https://link.springer.com/referenceworkentry/10.1007/3-540-29623-9_4410.

[31] T. Weinert, P. Skopintsev, D. James, F. Dworkowski, E. Panepucci, D. Kekilli, A. Furrer, S. Brünle, S. Mous, D. Ozerov, P. Nogly, M. Wang, and J. Standfuss, "Proton uptake mechanism in bacteriorhodopsin captured by serial synchrotron crystallography," *Science*, vol. 364, no. 6448, pp. 61–65, Jul. 2019, ISSN: 10959203. DOI: 10.1126/science.aaw8634. [Online]. Available: https://www.science.org.

[32] J. Sasaki and J. L. Spudich, "Proton Circulation During the Photocycle of Sensory Rhodopsin II," *Biophysical Journal*, vol. 77, no. 4, pp. 2145–2152, Oct. 1999, ISSN: 0006-3495. DOI: 10.1016/S0006-3495(99)77055-4. [Online]. Available: http://www.cell.com/article/S0006349599770554/fulltexthttp://www.cell.com/article/S0006349599770554/abstracthttps://www.cell.com/biophysj/abstract/S0006-3495(99)77055-4.

[33] G. Dai, X. Geng, Chaoluomeng, J. Tamogami, T. Kikukawa, M. Demura, N. Kamo, and T. Iwasa, "Photocycle of Sensory Rhodopsin II from Halobacterium salinarum (HsSRII): Mutation of D103 Accelerates M Decay and Changes the Decay Pathway of a 13-cis O-like Species," *Photochemistry and Photobiology*, vol. 94, no. 4, pp. 705–714, Jul. 2018, ISSN: 1751-1097. DOI: 10.1111/PHP.12917. [Online]. Available: https://onlinelibrary-wiley-com.ezproxy.ub.gu.se/doi/full/10.1111/php.12917https://onlinelibrary-wiley-com.ezproxy.ub.gu.se/doi/abs/10.1111/php.12917https://onlinelibrary-wiley-com.ezproxy.ub.gu.se/doi/10.1111/php.12917.

[34] R. Ashwini, S. Vijayanand, and J. Hemapriya, "Photonic Potential of Haloarchaeal Pigment Bacteriorhodopsin for Future Electronics: A Review," *Current Microbiology*, vol. 74, no. 8, pp. 996–1002, Aug. 2017, ISSN: 14320991. DOI: 10.1007/S00284-017-1271-5.

[35] I. Gushchin, A. Reshetnyak, V. Borshchevskiy, A. Ishchenko, E. Round, S. Grudinin, M. Engelhard, G. Büldt, and V. Gordeliy, "Active State of Sensory Rhodopsin II: Structural Determinants for Signal Transfer and Proton Pumping," *Journal of Molecular Biology*, vol. 412, no. 4, pp. 591–600, Sep. 2011, ISSN: 0022-2836. DOI: 10.1016/J.JMB.2011.07.022.

[36] Y. Sudo, M. Iwamoto, K. Shimono, and N. Kamo, "Pharaonis Phoborhodopsin Binds to its Cognate Truncated Transducer Even in the Presence of a Detergent with a 1:1 Stoichiometry¶," *Photochemistry and Photobiology*, vol. 74, no. 3, pp. 489–494, May 2007. DOI: 10.1562/0031-8655(2001)0740489PPBTIC2.0.CO2.

[37] A. A. Wegener, I. Chizhov, M. Engelhard, and H. J. Steinhoff, "Time-resolved detection of transient movement of helix F in spin-labelled pharaonis sensory rhodopsin II," *Journal of Molecular Biology*, vol. 301, no. 4, pp. 881–891, Aug. 2000, ISSN: 0022-2836. DOI: 10.1006/JMBI.2000.4008.

[38] M. Lotti, D. Porro, and F. Srienc, "Recombinant proteins and host cell physiology," *Journal of Biotechnology*, vol. 109, no. 1-2, pp. 1–2, Apr. 2004, ISSN: 0168-1656. DOI: 10.1016/J.JBIOTEC.2004.01.001.

[39] S. C. Almo and J. D. Love, "Better and faster: improvements and optimization for mammalian recombinant protein production," *Current Opinion in Structural Biology*, vol. 26, no. 1, pp. 39–43, Jun. 2014, ISSN: 0959-440X. DOI: 10.1016/J.SBI.2014.03.006.

[40] K. Hedfalk, "Further advances in the production of membrane proteins in Pichia pastoris," *http://dx.doi.org/10.4161/bioe.23886*, vol. 4, no. 6, pp. 363–367, 2013. DOI: 10.4161/BIOE.23886. [Online]. Available: https://www.tandfonline.com/doi/abs/10.4161/bioe.23886.

[41] G. L. Rosano and E. A. Ceccarelli, "Recombinant protein expression in Escherichia coli: advances and challenges," *Frontiers in Microbiology*, vol. 0, no. APR, p. 172, 2014, ISSN: 1664-302X. DOI: 10.3389/FMICB.2014.00172.

[42] T. A. Gomes, C. M. Zanette, and M. R. Spier, "An overview of cell disruption methods for intracellular biomolecules recovery," *https://doi-org.ezproxy.ub.gu.se/10.1080/10826068.2020.1728696*, vol. 50, no. 7, pp. 635–654, Aug. 2020. DOI: 10.1080/10826068.2020.1728696. [Online]. Available: https://www-tandfonline-com.ezproxy.ub.gu.se/doi/abs/10.1080/10826068.2020.1728696.

[43] M. S. Islam, A. Aryasomayajula, and P. R. Selvaganapathy, "A Review on Macroscale and Microscale Cell Lysis Methods," *Micromachines*, vol. 8, no. 3, 2017. DOI: 10.3390/MI8030083. [Online]. Available: /pmc/articles/PMC6190294//pmc/articles/PMC6190294/?report=abstracthttps://www.ncbi.nlm.nih.gov/pmc/articles/PMC6190294/.

[44] E. Grigorov, B. Kirov, M. B. Marinov, and V. Galabov, "Review of Microfluidic Methods for Cellular Lysis," *Micromachines*, vol. 12, no. 5, May 2021. DOI: 10.3390/MI12050498. [Online]. Available: /pmc/articles/PMC8145176//pmc/articles/PMC8145176/

?report=abstracthttps://www.ncbi.nlm.nih.gov/pmc/articles/PMC8145176/.

[45] K. Duquesne, V. Prima, and J. N. Sturgis, "Membrane Protein Solubilization and Composition of Protein Detergent Complexes," *Methods in Molecular Biology*, vol. 1432, pp. 243–260, Aug. 2016. DOI: 10.1007/978-1-4939-3637-3{_}15. [Online]. Available: https://link-springer-com.ezproxy.ub.gu.se/protocol/10.1007/978-1-4939-3637-3_15.

[46] O. Coskun, "Separation techniques: Chromatography," *Northern Clinics of Istanbul*, vol. 3, no. 2, p. 156, 2016. DOI: 10.14744/NCI.2016.32757. [Online]. Available: /pmc/articles/PMC5206469//pmc/articles/PMC5206469/?report=abstracthttps://www.ncbi.nlm.nih.gov/pmc/articles/PMC5206469/.

[47] L. Ling, L. W. Kao, and N. H. L. Wang, "A new general method for designing affinity chromatography processes," *Journal of Chromatography A*, vol. 1355, pp. 86–99, Aug. 2014, ISSN: 0021-9673. DOI: 10.1016/J.CHROMA.2014.05.081.

[48] R. R. Burgess, "A brief practical review of size exclusion chromatography: Rules of thumb, limitations, and troubleshooting," *Protein Expression and Purification*, vol. 150, pp. 81–85, Oct. 2018, ISSN: 1046-5928. DOI: 10.1016/J.PEP.2018.05.007.

[49] M. A. Dessau and Y. Modis, "Protein crystallization for X-ray crystallography," *Journal of Visualized Experiments*, no. 47, 2010, ISSN: 1940087X. DOI: 10.3791/2285. [Online]. Available: /pmc/articles/PMC3182643//pmc/articles/PMC3182643/?report=abstracthttps://www.ncbi.nlm.nih.gov/pmc/articles/PMC3182643/.

[50] C. G. Wermuth, D. Aldous, P. Raboisson, and D. Rognan, *The Practice of Medicinal Chemistry: Fourth Edition*. Elsevier Inc., Aug. 2015, pp. 1–458, ISBN: 9780124172050. DOI: 10.1016/C2012-0-03066-9.

[51] A. M. Glazer and G. Burns, "Space Groups for Solid State Scientists," *Space Groups for Solid State Scientists*, 2013. DOI: 10.1016/C2011-0-05712-5.

[52] S. Takahashi, K. Ohta, N. Furubayashi, B. Yan, M. Koga, Y. Wada, M. Yamada, K. Inaka, H. Tanaka, H. Miyoshi, T. Kobayashi, and S. Kamigaichi, "JAXA protein crystallization in space: ongoing improvements for growing high-quality crystals," *urn:issn:0909-0495*, vol. 20, no. 6, pp. 968–973, Sep. 2013, ISSN: 0909-0495. DOI: 10.1107/S0909049513021596. [Online]. Available: http://scripts.iucr.org/cgi-bin/paper?ys5094.

[53] I. Rayment, "Small-Scale Batch Crystallization of Proteins Revisited: An Underutilized Way to Grow Large Protein Crystals," *Structure*, vol. 10, no. 2, pp. 147–151, Feb. 2002, ISSN: 0969-2126. DOI: 10.1016/S0969-2126(02)00711-6.

[54] J. Holcomb, N. Spellmon, Y. Zhang, M. Doughan, C. Li, and Z. Yang, "Protein crystallization: Eluding the bottleneck of X-ray crystallography," *AIMS biophysics*, vol. 4, no. 4, p. 557, 2017. DOI: 10.3934/BIOPHY.2017.4.557. [Online]. Available: /pmc/articles/PMC5645037//pmc/articles/PMC5645037/?report=abstracthttps://www.ncbi.nlm.nih.gov/pmc/articles/PMC5645037/.

[55] V. Cherezov, "Lipidic cubic phase technologies for membrane protein structural studies," *Current Opinion in Structural Biology*, vol. 21, no. 4, pp. 559–566, Aug. 2011, ISSN: 0959-440X. DOI: 10.1016/J.SBI.2011.06.007.

[56] D. Li and M. Caffrey, "Structure and Functional Characterization of Membrane Integral Proteins in the Lipid Cubic Phase," *Journal of Molecular Biology*, vol. 432, no. 18, pp. 5104–5123, Aug. 2020, ISSN: 0022-2836. DOI: 10.1016/J.JMB.2020.02.024.

[57] M. Caffrey, "A comprehensive review of the lipid cubic phase or in meso method for crystallizing membrane and soluble proteins and complexes," *Acta Crystallographica. Section F, Structural Biology Communications*, vol. 71, no. Pt 1, p. 3, Jan. 2015, ISSN: 2053-230X. DOI: 10.1107/S2053230X14026843. [Online]. Available: http://www.ncbi.nlm.nih.gov/pubmed/25615961http://www.pubmedcentral.nih.gov/articlerender.fcgi?artid=PMC4304740.

[58] R. Andersson, C. Safari, P. Båth, R. Bosman, A. Shilova, P. Dahl, S. Ghosh, A. Dunge, R. Kjeldsen-Jensen, J. Nan, R. Shoeman, M. Kloos, R. Doak, U. Mueller, R. Neutze, and G. Brändén, "Well-based crystallization of lipidic cubic phase microcrystals for serial X-ray crystallography experiments," *urn:issn:2059-7983*, vol. 75, no. 10, pp. 937–946, Oct. 2019, ISSN: 2059-7983. DOI: 10.1107/S2059798319012695. [Online]. Available: http://scripts.iucr.org/cgi-bin/paper?nj5285https://journals.iucr.org/d/issues/2019/10/00/nj5285/.

[59] N. E. Chayen, "Comparative Studies of Protein Crystallization by Vapour-Diffusion and Microbatch Techniques," *Acta Crystallographica Section D*, vol. 54, no. 1, pp. 8–15, Jan. 1998, ISSN: 1399-0047. DOI: 10.1107/S0907444997005374. [Online]. Available: https://onlinelibrary.wiley.com/doi/full/10.1107/S0907444997005374https://onlinelibrary.wiley.com/doi/abs/10.1107/S0907444997005374https://onlinelibrary.wiley.com/doi/10.1107/S0907444997005374.

[60] A. McPherson, "Protein Crystallization," *Methods in Molecular Biology*, vol. 1607, pp. 17–50, 2017. DOI: 10.1007/978-1-4939-7000-1{_}2. [Online]. Available: https://link-springer-com.ezproxy.ub.gu.se/protocol/10.1007/978-1-4939-7000-1_2.

[61] L. Govada and N. E. Chayen, "Choosing the Method of Crystallization to Obtain Optimal Results," *Crystals 2019, Vol. 9, Page 106*, vol. 9, no. 2, p. 106, Feb. 2019. DOI: 10.3390/CRYST9020106. [Online]. Available: https://www.mdpi.com/2073-4352/9/2/106/htmhttps://www.mdpi.com/2073-4352/9/2/106.

[62] A. A. Chernov, "Protein crystals and their growth," *Journal of Structural Biology*, vol. 142, no. 1, pp. 3–21, Apr. 2003, ISSN: 1047-8477. DOI: 10.1016/S1047-8477(03)00034-0.

[63] M. Beckers, B. Weise, S. Kalapis, T. Gries, G. Seide, and C. A. Bunge, "Basics of light guidance," *Polymer Optical Fibres: Fibre Types, Materials, Fabrication, Characterisation and Applications*,

pp. 9–46, Jan. 2017. DOI: 10.1016/B978-0-08-100039-7.00002-6.

[64] L. M. Ailioaie and G. Litscher, *Molecular and cellular mechanisms of arthritis in children and adults: New perspectives on applied photobiomodulation*, Sep. 2020. DOI: 10.3390/ijms21186565. [Online]. Available: www.mdpi.com/journal/ijms.

[65] E. Mitchell, P. Kuhn, and E. Garman, "Demystifying the synchrotron trip: a first time user's guide," *Structure*, vol. 7, no. 5, R111–R121, May 1999, ISSN: 0969-2126. DOI: 10.1016/S0969-2126(99)80063-X. [Online]. Available: http://www.cell.com/article/S096921269980063X/fulltexthttp://www.cell.com/article/S096921269980063X/abstracthttps://www.cell.com/structure/abstract/S0969-2126(99)80063-X.

[66] R. Neutzo, R. Wouts, D. Van Der Spoel, E. Weckert, and J. Hajdu, "Potential for biomolecular imaging with femtosecond X-ray pulses," *Nature 2000 406:6797*, vol. 406, no. 6797, pp. 752–757, Aug. 2000, ISSN: 1476-4687. DOI: 10.1038/35021099. [Online]. Available: https://www-nature-com.ezproxy.ub.gu.se/articles/35021099.

[67] R. Neutze, "Opportunities and challenges for timeresolved studies of protein structural dynamics at X-ray free-electron lasers," *Philosophical Transactions of the Royal Society B: Biological Sciences*, vol. 369, no. 1647, Jul. 2014, ISSN: 14712970. DOI: 10.1098/rstb.2013.0318. [Online]. Available: http://dx.doi.org/10.1098/rstb.2013.0318.

[68] J. C. Spence, "XFELs for structure and dynamics in biology," *IUCrJ*, vol. 4, no. Pt 4, pp. 322–339, 2017, ISSN: 2052-2525. DOI: 10.1107/S2052252517005760. [Online]. Available: https://pubmed.ncbi.nlm.nih.gov/28875020/.

[69] R. Neutze and K. Moffat, "Time-resolved structural studies at synchrotrons and X-ray free electron lasers: opportunities and challenges.," *Current opinion in structural biology*, vol. 22, no. 5, pp. 651–9, Oct. 2012, ISSN: 1879-033X. DOI: 10.1016/j.sbi.2012.08.006. [Online]. Available: http://www.ncbi.nlm.nih.

gov/pubmed/23021004http://www.pubmedcentral.nih.gov/articlerender.fcgi?artid=PMC3520507.

[70] J. W. Pflugrath, "Practical macromolecular cryocrystallography," *Acta Crystallographica. Section F, Structural Biology Communications*, vol. 71, no. Pt 6, p. 622, Jun. 2015. DOI: 10.1107/S2053230X15008304. [Online]. Available: /pmc/articles/PMC4461322/ /pmc/articles/PMC4461322/?report=abstracthttps://www.ncbi.nlm.nih.gov/pmc/articles/PMC4461322/.

[71] T. Weinert, N. Olieric, R. Cheng, S. Brünle, D. James, D. Ozerov, D. Gashi, L. Vera, M. Marsh, K. Jaeger, F. Dworkowski, E. Panepucci, S. Basu, P. Skopintsev, A. S. Doré, T. Geng, R. M. Cooke, M. Liang, A. E. Prota, V. Panneels, P. Nogly, U. Ermler, G. Schertler, M. Hennig, M. O. Steinmetz, M. Wang, and J. Standfuss, "Serial millisecond crystallography for routine room-temperature structure determination at synchrotrons," *Nature Communications*, vol. 8, no. 1, p. 542, Dec. 2017, ISSN: 2041-1723. DOI: 10.1038/s41467-017-00630-4. [Online]. Available: http://www.nature.com/articles/s41467-017-00630-4.

[72] G. Brändén and R. Neutze, "Advances and challenges in time-resolved macromolecular crystallography," *Science*, vol. 373, no. 6558, Aug. 2021. DOI: 10.1126/SCIENCE.ABA0954. [Online]. Available: https://www.science.org/doi/abs/10.1126/science.aba0954.

[73] P. Fromme, W. S. Graves, and J. M. Martin-Garcia, "Serial Femtosecond Crystallography: A Decade at the Forefront in Structural Biology," *eLS*, pp. 1–17, May 2020. DOI: 10.1002/9780470015902.A0028964. [Online]. Available: https://onlinelibrary.wiley.com/doi/full/10.1002/9780470015902.a0028964https://onlinelibrary.wiley.com/doi/abs/10.1002/9780470015902.a0028964https://onlinelibrary.wiley.com/doi/10.1002/9780470015902.a0028964.

[74] H. N. Chapman, P. Fromme, A. Barty, T. A. White, R. A. Kirian, A. Aquila, M. S. Hunter, J. Schulz, D. P. Deponte, U. Weierstall, R. B. Doak, F. R. Maia, A. V. Martin, I. Schlichting, L. Lomb, N.

Coppola, R. L. Shoeman, S. W. Epp, R. Hartmann, D. Rolles, A. Rudenko, L. Foucar, N. Kimmel, G. Weidenspointner, P. Holl, M. Liang, M. Barthelmess, C. Caleman, S. Boutet, M. J. Bogan, J. Krzywinski, C. Bostedt, S. Bajt, L. Gumprecht, B. Rudek, B. Erk, C. Schmidt, A. Hömke, C. Reich, D. Pietschner, L. Ströder, G. Hauser, H. Gorke, J. Ullrich, S. Herrmann, G. Schaller, F. Schopper, H. Soltau, K. U. Kühnel, M. Messerschmidt, J. D. Bozek, S. P. Hau-Riege, M. Frank, C. Y. Hampton, R. G. Sierra, D. Starodub, G. J. Williams, J. Hajdu, N. Timneanu, M. M. Seibert, J. Andreasson, A. Rocker, O. Jönsson, M. Svenda, S. Stern, K. Nass, R. Andritschke, C. D. Schröter, F. Krasniqi, M. Bott, K. E. Schmidt, X. Wang, I. Grotjohann, J. M. Holton, T. R. Barends, R. Neutze, S. Marchesini, R. Fromme, S. Schorb, D. Rupp, M. Adolph, T. Gorkhover, I. Andersson, H. Hirsemann, G. Potdevin, H. Graafsma, B. Nilsson, and J. C. Spence, "Femtosecond X-ray protein nanocrystallography," *Nature*, vol. 470, no. 7332, pp. 73–78, Feb. 2011, ISSN: 1476-4687. DOI: 10.1038/NATURE09750. [Online]. Available: https://pubmed.ncbi.nlm.nih.gov/21293373/.

[75] U. Weierstall, D. James, C. Wang, T. A. White, D. Wang, W. Liu, J. C. Spence, R. Bruce Doak, G. Nelson, P. Fromme, R. Fromme, I. Grotjohann, C. Kupitz, N. A. Zatsepin, H. Liu, S. Basu, D. Wacker, G. Won Han, V. Katritch, S. Boutet, M. Messerschmidt, G. J. Williams, J. E. Koglin, M. Marvin Seibert, M. Klinker, C. Gati, R. L. Shoeman, A. Barty, H. N. Chapman, R. A. Kirian, K. R. Beyerlein, R. C. Stevens, D. Li, S. T. Shah, N. Howe, M. Caffrey, and V. Cherezov, "Lipidic cubic phase injector facilitates membrane protein serial femtosecond crystallography," *Nature Communications 2014 5:1*, vol. 5, no. 1, pp. 1–6, Feb. 2014, ISSN: 2041-1723. DOI: 10.1038/ncomms4309. [Online]. Available: https://www.nature.com/articles/ncomms4309.

[76] A. Shilova, H. Lebrette, O. Aurelius, J. Nan, M. Welin, R. Kovacic, S. Ghosh, C. Safari, R. J. Friel, M. Milas, Z. Matej, M. Hogbom, G. Branden, M. Kloos, R. L. Shoeman, B. Doak, T. Ursby, M. Hakansson, D. T. Logan, and U. Mueller, "Current status and

future opportunities for serial crystallography at MAX IV Laboratory," *Journal of Synchrotron Radiation*, vol. 27, no. Pt 5, p. 1095, Sep. 2020, ISSN: 16005775. DOI: 10.1107/S1600577520008735. [Online]. Available: /pmc/articles/PMC7467353//pmc/articles/PMC7467353/?report=abstracthttps://www.ncbi.nlm.nih.gov/pmc/articles/PMC7467353/.

[77] J. Tenboer, S. Basu, N. Zatsepin, K. Pande, D. Milathianaki, M. Frank, M. Hunter, S. Boutet, G. J. Williams, J. E. Koglin, D. Oberthuer, M. Heymann, C. Kupitz, C. Conrad, J. Coe, S. Roy-Chowdhury, U. Weierstall, D. James, D. Wang, T. Grant, A. Barty, O. Yefanov, J. Scales, C. Gati, C. Seuring, V. Srajer, R. Henning, P. Schwander, R. Fromme, A. Ourmazd, K. Moffat, J. J. Van Thor, J. C. H. Spence, P. Fromme, H. N. Chapman, and M. Schmidt, "Time-resolved serial crystallography captures high-resolution intermediates of photoactive yellow protein," *Science*, vol. 346, no. 6214, 1242 LP –1246, Dec. 2014. [Online]. Available: http://science.sciencemag.org/content/346/6214/1242.abstract.

[78] H. R. Powell, "A beginner's guide to X-ray data processing," *The Biochemist*, vol. 43, no. 3, pp. 46–50, Jun. 2021, ISSN: 0954-982X. DOI: 10.1042/BIO{_}2021{_}124. [Online]. Available: /biochemist/article/43/3/46/228828/A-beginner-s-guide-to-X-ray-data-processing.

[79] K. M. Dalton, J. B. Greisman, and D. R. Hekstra, "CARELESS: A VARIATIONAL BAYESIAN MODEL FOR MERGING X-RAY DIFFRACTION DATA A PREPRINT," *bioRxiv*, p. 2021.01.05.425510, Jan. 2021. DOI: 10.1101/2021.01.05.425510. [Online]. Available: https://doi.org/10.1101/2021.01.05.425510.

[80] G. L. Taylor, "Introduction to phasing," *Acta Crystallographica Section D: Biological Crystallography*, vol. 66, no. Pt 4, p. 325, 2010, ISSN: 09074449. DOI: 10.1107/S0907444910006694. [Online]. Available: /pmc/articles/PMC2852296//pmc/articles/PMC2852296/?report=abstracthttps://www.ncbi.nlm.nih.gov/pmc/articles/PMC2852296/.

[81] G. Brändén and R. Neutze, "Advances and challenges in time-resolved macromolecular crystallography," *Science*, vol. 373, no. 6558, Aug. 2021, ISSN: 10959203. DOI: 10.1126/SCIENCE.ABA0954.

[82] M. Cammarata, M. Levantino, F. Schotte, P. A. Anfinrud, F. Ewald, J. Choi, A. Cupane, M. Wulff, and H. Ihee, "Tracking the structural dynamics of proteins in solution using time-resolved wide-angle X-ray scattering," *Nature Methods*, vol. 5, no. 10, pp. 881–886, Oct. 2008, ISSN: 1548-7091. DOI: 10.1038/nmeth.1255. [Online]. Available: http://www.nature.com/articles/nmeth.1255.

[83] P. Nogly, T. Weinert, D. James, S. Carbajo, D. Ozerov, A. Furrer, D. Gashi, V. Borin, P. Skopintsev, K. Jaeger, K. Nass, P. Båth, R. Bosman, J. Koglin, M. Seaberg, T. Lane, D. Kekilli, S. Brünle, T. Tanaka, W. Wu, C. Milne, T. White, A. Barty, U. Weierstall, V. Panneels, E. Nango, S. Iwata, M. Hunter, I. Schapiro, G. Schertler, R. Neutze, and J. Standfuss, "Retinal isomerization in bacteriorhodopsin captured by a femtosecond x-ray laser," *Science*, vol. 361, no. 6398, Jul. 2018, ISSN: 10959203. DOI: 10.1126/SCIENCE.AAT0094.

[84] J. L. Spudich, O. A. Sineshchekov, and E. G. Govorunova, "Mechanism divergence in microbial rhodopsins," *Biochimica et Biophysica Acta (BBA) - Bioenergetics*, vol. 1837, no. 5, pp. 546–552, May 2014, ISSN: 0005-2728. DOI: 10.1016/J.BBABIO.2013.06.006.

[85] E. Pebay-Peyroula, G. Rummel, J. P. Rosenbusch, and E. M. Landau, "X-ray Structure of Bacteriorhodopsin at 2.5 Angstroms from Microcrystals Grown in Lipidic Cubic Phases," *Science*, vol. 277, no. 5332, pp. 1676–1681, Sep. 1997, ISSN: 00368075. DOI: 10.1126/SCIENCE.277.5332.1676. [Online]. Available: https://www.science.org/doi/abs/10.1126/science.277.5332.1676.

[86] I. P. Hohenfeld, A. A. Wegener, and M. Engelhard, "Purification of histidine tagged bacteriorhodopsin, pharaonis halorhodopsin and pharaonis sensory rhodopsin II functionally expressed in Escherichia coli," *FEBS Letters*, vol. 442, no. 2-3, pp. 198–202, Jan. 1999,

ISSN: 1873-3468. DOI: 10.1016/S0014-5793(98)01659-7. [Online]. Available: https://onlinelibrary.wiley.com/doi/full/10.1016/S0014-5793%2898%2901659-7https://onlinelibrary.wiley.com/doi/abs/10.1016/S0014-5793%2898%2901659-7https://febs.onlinelibrary.wiley.com/doi/10.1016/S0014-5793(98)01659-7.

[87] D. Li and M. Caffrey, "Lipid cubic phase as a membrane mimetic for integral membrane protein enzymes," *Proceedings of the National Academy of Sciences of the United States of America*, vol. 108, no. 21, pp. 8639–8644, May 2011, ISSN: 00278424. DOI: 10.1073/PNAS.1101815108/-/DCSUPPLEMENTAL. [Online]. Available: /pmc/articles/PMC3102357//pmc/articles/PMC3102357/?report=abstracthttps://www.ncbi.nlm.nih.gov/pmc/articles/PMC3102357/.

[88] T. A. White, R. A. Kirian, A. V. Martin, A. Aquila, K. Nass, A. Barty, and H. N. Chapman, "CrystFEL: a software suite for snapshot serial crystallography," *urn:issn:0021-8898*, vol. 45, no. 2, pp. 335–341, Mar. 2012, ISSN: 0021-8898. DOI: 10.1107/S0021889812002312. [Online]. Available: http://scripts.iucr.org/cgi-bin/paper?db5097.

[89] P. D. Adams, P. V. Afonine, G. Bunkóczi, V. B. Chen, N. Echols, J. J. Headd, L. W. Hung, S. Jain, G. J. Kapral, R. W. Grosse Kunstleve, A. J. McCoy, N. W. Moriarty, R. D. Oeffner, R. J. Read, D. C. Richardson, J. S. Richardson, T. C. Terwilliger, and P. H. Zwart, "The Phenix software for automated determination of macromolecular structures," *Methods*, vol. 55, no. 1, pp. 94–106, Sep. 2011, ISSN: 1046-2023. DOI: 10.1016/J.YMETH.2011.07.005.

[90] C. Wickstrand, G. Katona, T. Nakane, P. Nogly, J. Standfuss, E. Nango, and R. Neutze, "A tool for visualizing protein motions in time-resolved crystallography," *Structural Dynamics*, vol. 7, no. 2, p. 024 701, Apr. 2020, ISSN: 23297778. DOI: 10.1063/1.5126921. [Online]. Available: https://aca.scitation.org/doi/abs/10.1063/1.5126921.

[91] K. Edman, A. Royant, P. Nollert, C. A. Maxwell, E. Pebay-Peyroula, J. Navarro, R. Neutze, and E. M. Landau, "Early structural rearrangements in the photocycle of an integral membrane sensory receptor," *Structure (London, England : 1993)*, vol. 10, no. 4, pp. 473–482, 2002, ISSN: 0969-2126. DOI: 10.1016/S0969-2126(02)00736-0. [Online]. Available: https://pubmed.ncbi.nlm.nih.gov/11937052/.

[92] K. Shimono, T. Hayashi, Y. Ikeura, Y. Sudo, M. Iwamoto, and N. Kamo, "Importance of the Broad Regional Interaction for Spectral Tuning in Natronobacterium pharaonis Phoborhodopsin (Sensory Rhodopsin II)," *Journal of Biological Chemistry*, vol. 278, no. 26, pp. 23 882–23 889, Jun. 2003, ISSN: 0021-9258. DOI: 10.1074/JBC.M301200200.

[93] E. Nango, A. Royant, M. Kubo, T. Nakane, C. Wickstrand, T. Kimura, T. Tanaka, K. Tono, C. Song, R. Tanaka, T. Arima, A. Yamashita, J. Kobayashi, T. Hosaka, E. Mizohata, P. Nogly, M. Sugahara, D. Nam, T. Nomura, T. Shimamura, D. Im, T. Fujiwara, Y. Yamanaka, B. Jeon, T. Nishizawa, K. Oda, M. Fukuda, R. Andersson, P. Båth, R. Dods, J. Davidsson, S. Matsuoka, S. Kawatake, M. Murata, O. Nureki, S. Owada, T. Kameshima, T. Hatsui, Y. Joti, G. Schertler, M. Yabashi, A. N. Bondar, J. Standfuss, R. Neutze, and S. Iwata, "A three-dimensional movie of structural changes in bacteriorhodopsin," *Science (New York, N.Y.)*, vol. 354, no. 6319, pp. 1552–1557, Dec. 2016, ISSN: 1095-9203. DOI: 10.1126/SCIENCE.AAH3497. [Online]. Available: https://pubmed.ncbi.nlm.nih.gov/28008064/.

[94] M. Andersson, E. Malmerberg, S. Westenhoff, G. Katona, M. Cammarata, A. B. Wöhri, L. C. Johansson, F. Ewald, M. Eklund, M. Wulff, J. Davidsson, and R. Neutze, "Structural Dynamics of Light-Driven Proton Pumps," *Structure*, vol. 17, no. 9, pp. 1265–1275, Sep. 2009, ISSN: 09692126. DOI: 10.1016/j.str.2009.07.007. [Online]. Available: http://www.ncbi.nlm.nih.gov/pubmed/19748347http://www.sciencedirect.com/science/article/pii/S0969212609002901?via%3Dihub.

[95] N. Radzwill, K. Gerwert, and H. J. Steinhoff, "Time-Resolved Detection of Transient Movement of Helices F and G in Doubly Spin-Labeled Bacteriorhodopsin," *Biophysical Journal*, vol. 80, no. 6, pp. 2856–2866, Jun. 2001, ISSN: 0006-3495. DOI: 10.1016/S0006-3495(01)76252-2.

[96] J. P. Klare, E. Bordignon, M. Engelhard, and H. J. Steinhoff, "Sensory rhodopsin II and bacteriorhodopsin: light activated helix F movement," *Photochemical & photobiological sciences : Official journal of the European Photochemistry Association and the European Society for Photobiology*, vol. 3, no. 6, pp. 543–547, Jun. 2004, ISSN: 1474-905X. DOI: 10.1039/B402656J. [Online]. Available: https://pubmed.ncbi.nlm.nih.gov/15170483/.

[97] A. Ishchenko, E. Round, V. Borshchevskiy, S. Grudinin, I. Gushchin, J. P. Klare, T. Balandin, A. Remeeva, M. Engelhard, G. Büldt, and V. Gordeliy, "Ground state structure of D75N mutant of sensory rhodopsin II in complex with its cognate transducer," *Journal of photochemistry and photobiology. B, Biology*, vol. 123, pp. 55–58, Jun. 2013, ISSN: 1873-2682. DOI: 10.1016/J.JPHOTOBIOL.2013.03.008. [Online]. Available: https://pubmed.ncbi.nlm.nih.gov/23619282/.

[98] S. French and K. Wilson, "On the treatment of negative intensity observations," *urn:issn:0567-7394*, vol. 34, no. 4, pp. 517–525, Jul. 1978, ISSN: 0567-7394. DOI: 10.1107/S0567739478001114. [Online]. Available: //scripts.iucr.org/cgi-bin/paper?a15572.

[99] T. C. Terwilliger, F. Di Maio, R. J. Read, D. Baker, G. Bunkóczi, P. D. Adams, R. W. Grosse-Kunstleve, P. V. Afonine, and N. Echols, "Phenix.mr-rosetta: Molecular replacement and model rebuilding with Phenix and Rosetta," *Journal of Structural and Functional Genomics*, vol. 13, no. 2, pp. 81–90, Jun. 2012, ISSN: 1345711X. DOI: 10.1007/s10969-012-9129-3. [Online]. Available: www.phenix-online.org.

[100] P. Emsley and K. Cowtan, "Coot: Model-building tools for molecular graphics," *Acta Crystallographica Section D: Biological Crystallography*, vol. 60, no. 12 I, pp. 2126–2132, Dec. 2004, ISSN: 09074449. DOI: 10.1107/S0907444904019158/HTTPS://JOURNALS.IUCR.ORG/SERVICES/CONTACTUS.HTML. [Online]. Available: //scripts.iucr.org/cgi-bin/paper?ba5070.

[101] V. I. Gordeliy, R. Schlesinger, R. Efremov, G. Büldt, and J. Heberle, "Crystallization in Lipidic Cubic Phases," in *Membrane Protein Protocols: Expression, Purification, and Characterization*, B. S. Selinsky, Ed., Totowa, NJ: Humana Press, 2003, pp. 305–316.

[102] Y. Sudo, M. Iwamoto, K. Shimono, and N. Kamo, "Tyr-199 and Charged Residues of pharaonis PhoborhodopsinAre Important for the Interaction with its Transducer," *Biophysical Journal*, vol. 83, no. 1, pp. 427–432, Jul. 2002, ISSN: 0006-3495. DOI: 10.1016/S0006-3495(02)75180-1.

[103] A. A. Wegener, J. P. Klare, M. Engelhard, and H. J. Steinhoff, "Structural insights into the early steps of receptor–transducer signal transfer in archaeal phototaxis," *The EMBO Journal*, vol. 20, no. 19, p. 5312, Oct. 2001, ISSN: 02614189. DOI: 10.1093/EMBOJ/20.19.5312. [Online]. Available: /pmc/articles/PMC125640/ /pmc/articles/PMC125640/?report=abstracthttps://www.ncbi.nlm.nih.gov/pmc/articles/PMC125640/.

[104] M. Etzkorn, K. Seidel, L. Li, S. Martell, M. Geyer, M. Engelhard, and M. Baldus, "Complex formation and light activation in membrane-embedded sensory rhodopsin II as seen by solid-state NMR spectroscopy," *Structure (London, England : 1993)*, vol. 18, no. 3, pp. 293–300, Mar. 2010, ISSN: 1878-4186. DOI: 10.1016/J.STR.2010.01.011. [Online]. Available: https://pubmed.ncbi.nlm.nih.gov/20223212/.

[105] E. Bordignon, J. P. Klare, M. Doebber, A. A. Wegener, S. Martell, M. Engelhard, and H. J. Steinhoff, "Structural analysis of a HAMP domain: The linker region of the phototransducer in complex with sensory rhodopsin II," *Journal of Biological Chemistry*, vol. 280,

no. 46, pp. 38 767–38 775, 2005, ISSN: 00219258. DOI: 10.1074/JBC.M509391200.

[106] T. R. Schneider, "Objective comparison of protein structures: error-scaled difference distance matrices," *Acta crystallographica. Section D, Biological crystallography*, vol. 56, no. Pt 6, pp. 714–721, 2000, ISSN: 0907-4449. DOI: 10.1107/S0907444900003723. [Online]. Available: https://pubmed.ncbi.nlm.nih.gov/10818348/.

[107] C. Wickstrand, R. Dods, A. Royant, and R. Neutze, "Bacteriorhodopsin: Would the real structural intermediates please stand up?" *Biochimica et Biophysica Acta (BBA) - General Subjects*, vol. 1850, no. 3, pp. 536–553, Mar. 2015, ISSN: 0304-4165. DOI: 10.1016/J.BBAGEN.2014.05.021.

[108] I. Gushchin and V. Gordeliy, "Transmembrane Signal Transduction in Two-Component Systems: Piston, Scissoring, or Helical Rotation?" *BioEssays : news and reviews in molecular, cellular and developmental biology*, vol. 40, no. 2, Feb. 2018, ISSN: 1521-1878. DOI: 10.1002/BIES.201700197. [Online]. Available: https://pubmed.ncbi.nlm.nih.gov/29280502/.

[109] J. Wang, J. Sasaki, A. L. Tsai, and J. L. Spudich, "HAMP Domain Signal Relay Mechanism in a Sensory Rhodopsin-Transducer Complex," *The Journal of Biological Chemistry*, vol. 287, no. 25, p. 21 316, Jun. 2012, ISSN: 00219258. DOI: 10.1074/JBC.M112.344622. [Online]. Available: /pmc/articles/PMC3375552//pmc/articles/PMC3375552/?report=abstracthttps://www.ncbi.nlm.nih.gov/pmc/articles/PMC3375552/.

[110] Y. L. Ryzhykau, P. S. Orekhov, M. I. Rulev, A. V. Vlasov, I. A. Melnikov, D. A. Volkov, M. Y. Nikolaev, D. V. Zabelskii, T. N. Murugova, V. V. Chupin, A. V. Rogachev, A. Y. Gruzinov, D. I. Svergun, M. E. Brennich, I. Y. Gushchin, M. Soler-Lopez, A. Bothe, G. Büldt, G. Leonard, M. Engelhard, A. I. Kuklin, and V. I. Gordeliy, "Molecular model of a sensor of two-component signaling system," *Scientific Reports 2021 11:1*, vol. 11, no. 1, pp. 1–15, May 2021, ISSN: 2045-2322. DOI: 10.1038/s41598-021-89613-6. [Online].

Available: https://www.nature.com/articles/s41598-021-89613-6.

[111] E. Nango, A. Royant, M. Kubo, T. Nakane, C. Wickstrand, T. Kimura, T. Tanaka, K. Tono, C. Song, R. Tanaka, T. Arima, A. Yamashita, J. Kobayashi, T. Hosaka, E. Mizohata, P. Nogly, M. Sugahara, D. Nam, T. Nomura, T. Shimamura, D. Im, T. Fujiwara, Y. Yamanaka, B. Jeon, T. Nishizawa, K. Oda, M. Fukuda, R. Andersson, P. Båth, R. Dods, J. Davidsson, S. Matsuoka, S. Kawatake, M. Murata, O. Nureki, S. Owada, T. Kameshima, T. Hatsui, Y. Joti, G. Schertler, M. Yabashi, A. N. Bondar, J. Standfuss, R. Neutze, and S. Iwata, "A three-dimensional movie of structural changes in bacteriorhodopsin," *Science (New York, N.Y.)*, vol. 354, no. 6319, pp. 1552–1557, Dec. 2016, ISSN: 1095-9203. DOI: 10.1126/SCIENCE.AAH3497. [Online]. Available: https://pubmed.ncbi.nlm.nih.gov/28008064/.

[112] P. Nogly, T. Weinert, D. James, S. Carbajo, D. Ozerov, A. Furrer, D. Gashi, V. Borin, P. Skopintsev, K. Jaeger, K. Nass, P. Båth, R. Bosman, J. Koglin, M. Seaberg, T. Lane, D. Kekilli, S. Brünle, T. Tanaka, W. Wu, C. Milne, T. White, A. Barty, U. Weierstall, V. Panneels, E. Nango, S. Iwata, M. Hunter, I. Schapiro, G. Schertler, R. Neutze, and J. Standfuss, "Retinal isomerization in bacteriorhodopsin captured by a femtosecond x-ray laser.," *Science (New York, N.Y.)*, vol. 361, no. 6398, eaat0094, Jul. 2018, ISSN: 1095-9203. DOI: 10.1126/science.aat0094. [Online]. Available: http://www.ncbi.nlm.nih.gov/pubmed/29903883.

[113] C. Wickstrand, P. Nogly, E. Nango, S. Iwata, J. Standfuss, and R. Neutze, "Bacteriorhodopsin: Structural Insights Revealed Using X-Ray Lasers and Synchrotron Radiation," *Annual review of biochemistry*, vol. 88, pp. 59–83, Jun. 2019, ISSN: 1545-4509. DOI: 10.1146/ANNUREV-BIOCHEM-013118-111327. [Online]. Available: https://pubmed.ncbi.nlm.nih.gov/30830799/.

[114] K. Oda, T. Nomura, T. Nakane, K. Yamashita, K. Inoue, S. Ito, J. Vierock, K. Hirata, A. D. Maturana, K. Katayama, T. Ikuta, I. Ishigami, T. Izume, R. Umeda, R. Eguma, S. Oishi, G. Kasuya, T. Kato, T. Kusakizako, W. Shihoya, H. Shimada, T. Takatsuji, M.

Takemoto, R. Taniguchi, A. Tomita, R. Nakamura, M. Fukuda, H. Miyauchi, Y. Lee, E. Nango, R. Tanaka, T. Tanaka, M. Sugahara, T. Kimura, T. Shimamura, T. Fujiwara, Y. Yamanaka, S. Owada, Y. Joti, K. Tono, R. Ishitani, S. Hayashi, H. Kandori, P. Hegemann, S. Iwata, M. Kubo, T. Nishizawa, and O. Nureki, "Time-resolved serial femtosecond crystallography reveals early structural changes in channelrhodopsin," *eLife*, vol. 10, Mar. 2021, ISSN: 2050084X. DOI: 10.7554/ELIFE.62389.

[115] H. Takala, A. Björling, O. Berntsson, H. Lehtivuori, S. Niebling, M. Hoernke, I. Kosheleva, R. Henning, A. Menzel, J. A. Ihalainen, and S. Westenhoff, "Signal amplification and transduction in phytochrome photosensors," *Nature 2014 509:7499*, vol. 509, no. 7499, pp. 245–248, Apr. 2014, ISSN: 1476-4687. DOI: 10.1038/nature13310. [Online]. Available: https://www.nature.com/articles/nature13310.

[116] D. Arnlund, L. C. Johansson, C. Wickstrand, A. Barty, G. J. Williams, E. Malmerberg, J. Davidsson, D. Milathianaki, D. P. DePonte, R. L. Shoeman, D. Wang, D. James, G. Katona, S. Westenhoff, T. A. White, A. Aquila, S. Bari, P. Berntsen, M. Bogan, T. B. Van Driel, R. B. Doak, K. S. Kjær, M. Frank, R. Fromme, I. Grotjohann, R. Henning, M. S. Hunter, R. A. Kirian, I. Kosheleva, C. Kupitz, M. Liang, A. V. Martin, M. M. Nielsen, M. Messerschmidt, M. M. Seibert, J. Sjöhamn, F. Stellato, U. Weierstall, N. A. Zatsepin, J. C. Spence, P. Fromme, I. Schlichting, S. Boutet, G. Groenhof, H. N. Chapman, and R. Neutze, "Visualizing a protein quake with time-resolved X-ray scattering at a free-electron laser," *Nature Methods 2014 11:9*, vol. 11, no. 9, pp. 923–926, Aug. 2014, ISSN: 1548-7105. DOI: 10.1038/nmeth.3067. [Online]. Available: https://www.nature.com/articles/nmeth.3067.

[117] A. Björling, O. Berntsson, H. Lehtivuori, H. Takala, A. J. Hughes, M. Panman, M. Hoernke, S. Niebling, L. Henry, R. Henning, I. Kosheleva, V. Chukharev, N. V. Tkachenko, A. Menzel, G. Newby, D. Khakhulin, M. Wulff, J. A. Ihalainen, and S. Westenhoff, "Structural photoactivation of a full-length bacterial phytochrome," *Science Advances*, vol. 2, no. 8, Aug. 2016, ISSN: 23752548. DOI: 10.

1126/SCIADV.1600920/SUPPL{_}FILE/1600920{_}SM.PDF. [Online]. Available: https://www.science.org/doi/full/10.1126/sciadv.1600920.

[118] S. Niebling, A. Björling, and S. Westenhoff, "MARTINI bead form factors for the analysis of time-resolved X-ray scattering of proteins," *Journal of applied crystallography*, vol. 47, no. Pt 4, pp. 1190–1198, 2014, ISSN: 0021-8898. DOI: 10.1107/S1600576714009959. [Online]. Available: https://pubmed.ncbi.nlm.nih.gov/25242909/.

[119] P. L. Ramachandran, J. E. Lovett, P. J. Carl, M. Cammarata, J. H. Lee, Y. O. Jung, H. Ihee, C. R. Timmel, and J. J. Van Thor, "The short-lived signaling state of the photoactive yellow protein photoreceptor revealed by combined structural probes," *Journal of the American Chemical Society*, vol. 133, no. 24, pp. 9395–9404, Jun. 2011, ISSN: 1520-5126. DOI: 10.1021/JA200617T. [Online]. Available: https://pubmed.ncbi.nlm.nih.gov/21627157/.

[120] K. H. Kim, S. Muniyappan, K. Y. Oang, J. G. Kim, S. Nozawa, T. Sato, S. Y. Koshihara, R. Henning, I. Kosheleva, H. Ki, Y. Kim, T. W. Kim, J. Kim, S. I. Adachi, and H. Ihee, "Direct observation of cooperative protein structural dynamics of homodimeric hemoglobin from 100 ps to 10 ms with pump-probe X-ray solution scattering," *Journal of the American Chemical Society*, vol. 134, no. 16, pp. 7001–7008, Apr. 2012, ISSN: 00027863. DOI: 10.1021/JA210856V/SUPPL{_}FILE/JA210856V{_}SI{_}001.PDF. [Online]. Available: https://pubs.acs.org/doi/full/10.1021/ja210856v.

[121] M. Levantino, G. Schirò, H. T. Lemke, G. Cottone, J. M. Glownia, D. Zhu, M. Chollet, H. Ihee, A. Cupane, and M. Cammarata, "Ultrafast myoglobin structural dynamics observed with an X-ray free-electron laser," *Nature Communications*, 2015, ISSN: 2041-1723. DOI: 10.1038/ncomms7772.

[122] S. Subramanlam and R. Henderson, "Molecular mechanism of vectorial proton translocation by bacteriorhodopsin," *Nature*, vol. 406, no. 6796, pp. 653–657, Aug. 2000, ISSN: 0028-0836. DOI: 10.

1038/35020614. [Online]. Available: https://pubmed.ncbi.nlm.nih.gov/10949309/.

[123] S. Pronk, S. Páll, R. Schulz, P. Larsson, P. Bjelkmar, R. Apostolov, M. R. Shirts, J. C. Smith, P. M. Kasson, D. Van Der Spoel, B. Hess, and E. Lindahl, "GROMACS 4.5: a high-throughput and highly parallel open source molecular simulation toolkit," *Bioinformatics (Oxford, England)*, vol. 29, no. 7, pp. 845–854, Apr. 2013, ISSN: 1367-4811. DOI: 10.1093/BIOINFORMATICS/BTT055. [Online]. Available: https://pubmed.ncbi.nlm.nih.gov/23407358/.

[124] D. Svergun, C. Barberato, and M. H. Koch, "CRYSOL – a Program to Evaluate X-ray Solution Scattering of Biological Macromolecules from Atomic Coordinates," *urn:issn:0021-8898*, vol. 28, no. 6, pp. 768–773, Dec. 1995, ISSN: 0021-8898. DOI: 10.1107/S0021889895007047. [Online]. Available: //scripts.iucr.org/cgi-bin/paper?li5001.

[125] J. P. Klare and H. J. Steinhoff, "Spin labeling EPR," *Photosynthesis Research 2009 102:2*, vol. 102, no. 2, pp. 377–390, Aug. 2009, ISSN: 1573-5079. DOI: 10.1007/S11120-009-9490-7. [Online]. Available: https://link.springer.com/article/10.1007/s11120-009-9490-7.